Evaluation of the WRF model based on observations made by controlled meteorological balloons in the atmospheric boundary layer of Svalbard

Author:
Marina Lara Dütsch

Supervisor:
Lars Robert Hole

September 7, 2012

Abstract

In the period of 5 May 2011 to 12 May 2011, five controlled meteorological balloons were launched from Ny Ålesund on Svalbard. They measured vertical profiles over the coastal area in the vicinity of Ny Ålesund and over sea ice to the east of Svalbard. Together with timeseries measured by three meteorological research stations, the profiles measured by the balloons were used to evaluate the performance of the Weather Research and Forecasting model and in particular of three different boundary layer schemes applied in the model. The largest errors were found in the profiles over sea ice, where the model underestimated potential temperature and overestimated wind speed. Furthermore, the model showed difficulties in capturing temperature inversions and low level jets. The Quasi-Normal Scale Elimination scheme yielded the lowest errors and highest correlation for the timeseries, while the Yonsei University scheme achieved the best results for the vertical profiles.

Contents

1 Introduction

At high latitudes, global warming leads to surface temperatures increasing by a rate much higher than at low latitudes (3°C to 10°C at the North Pole compared to 2°C to 4°C in the tropics for a doubling of CO_2 (Lu and Cai, 2010)), a phenomenon which is known as polar amplification (PA). PA indicates a higher climate sensitivity of polar regions due to mechanisms such as the surface albedo feedback, increased poleward energy transport, water vapour feedback, cloud processes and damping of outgoing longwave radiation by thermal inversions, a.o. (Bintanja et al., 2011). It makes polar regions play a critical role in future climate projections.

However, the range of warming at high latitudes simulated in global climate models (GCMs) in response to increasing greenhouse gas concentrations is large (Houghton et al., 2001). The large spread can partly be explained by the lack of observational data for polar regions, which would be required to initialise and validate the model, as well as by the fact that the parameterisations applied in GCMs are often adapted to and validated against lower latitudes and might not necessarily be applicable to high latitudes. Furthermore, polar regions provide a rather complex area and therefore a challenge to numerical models: Advection of sea ice and thermodynamic ice formation, growth and melt can lead to high temporal and spatial variations in surface conditions. While the surface temperature of open water areas is practically at the freezing point of water (-1.8°C), the surface temperature of thick snow covered sea ice can be less than -40°C. Hence, the turbulent surface fluxes can vary by up to two orders of magnitude (Kilpeläinen et al., 2011). In addition, the stratification of the atmospheric boundary layer (ABL) over sea ice is usually strongly stable during winter, and weakly stable to neutral during summer (Persson et al., 2002). Strong stable stratification implies that effects of flows over small-scale topography, such as channelling, katabatic flows and mountain waves, are comparable to effects of flows over much higher topography during unstable stratification. Modelling of these effects would then require a much higher horizontal and vertical resolution (than currently available for GCMs).

To improve the understanding and modelling of the important physical processes taking place in polar regions, Regional Climate Models (RCMs) can help. They typically have a higher resolution and hence a better treatment of topography, land-sea mask and small-scale physical processes than GCMs. Moreover, the physics of the model can be optimised for polar conditions. Rinke et al. (2006) compared simulations of eight different RCMs over the Western Arctic for the period September 1997 - September 1998 (the year of the Surface Heat Budget of the Arctic Ocean (SHEBA) campaign) to European Center for Medium-Range Weather Forecasts (ECMWF) analyses. They found that the model ensemble mean in general agrees well with the ECMWF analyses. Yet, there was a large across-model scatter, especially for the 2m temperature over land, the surface

radiation fluxes and cloud cover, and mainly in the lowest model levels, which indicates a still high uncertainty in current Arctic RCM simulations.

In this study, we will verify the Weather Research and Forecasting (WRF) mesoscale model against profiles measured by controlled meteorological (CMET) balloons launched in May 2011 from Ny Ålesund on Svalbard. CMET balloons are unique in that their altitude can be controlled by operators on the ground via a satellite link. It is therefore possible to take vertical soundings at any time during the balloon flight. In addition, since no helium is released during the flight, the balloons are able to fly long and far, which gives us the opportunity to investigate areas far away from research bases. CMET balloons were developed at the Smith College, USA, and have been previously used by, e.g., Riddle et al. (2006), Voss et al. (2010) and Mentzoni (2011). Voss et al. (2010) investigated the evolving vertical structure of the polluted Mexico City Area outflow by making repeated balloon profile measurements of temperature, humidity and wind in the advecting outflow. Riddle et al. (2006) and Mentzoni (2011) used the CMET balloons as a tool to verify atmospheric trajectory models - namely FlexTra (Stohl et al., 1995) and FlexPart (Stohl et al., 1998) - in the United States and in the Arctic, respectively.

Due to the rather harsh conditions, which make it difficult to carry out field campaigns in polar regions, only few studies have been conducted that compare observations (in particular balloon measurements) to a mesoscale model in the Arctic. WRF has previously been evaluated against measurements from weather stations on Greenland, Svalbard and the Arctic Ocean. E.g., Hines and Bromwich (2008) validated a polar optimised version of WRF (Polar WRF) against measurements from automatic weather stations (AWS) on the Greenland ice sheet in June 2001 and December 2002. Bromwich et al. (2009) used the detailed measurements gained during the SHEBA program in 1997 - 1998 to evaluate the same model (Polar WRF) over the Arctic Ocean. Kilpeläinen et al. (2011) compared model results from the standard WRF model to tower observations and radiosoundings in three Svalbard fjords in winter and spring 2008. Livik (2011) evaluated WRF against measurements from AWS placed at several locations along Kongsfjorden, Svalbard, in spring 2010. Mäkiranta et al. (2011) compared WRF to mast measurements made in Wahlenbergfjorden, Svalbard, in May 2006 and April 2007, and Kilpeläinen et al. (2012) compared both polar and standard WRF to tethered balloon soundings and mast observations taken in March and April 2009. In addition, Mayer et al. (2012a) and Mayer et al. (2012b) used the recently developed small unmanned meteorological observer (SUMO), a remotely controlled model aircraft equipped with meteorological sensors, to investigate the performance of the WRF model over Iceland and over Svalbard.

In most of the studies, the ABL was either parameterised with the Yonsei University (YSU) Scheme, which is the default scheme in WRF, or the Mellor-Yamada-Janjic (MYJ) scheme, or both. Mayer et al. (2012b) and Kilpeläinen et al. (2012) additionally applied the Quasi-Normal Scale Elimination (QNSE) scheme, a new option in WRF

version 3, which showed a very good performance especially in the lower levels. In fact, Kilpeläinen et al. (2012) found that the QNSE scheme outperformed both the YSU and the MYJ scheme in overall agreement with the observations. The focus of this study is to investigate the performance of the YSU, the MYJ and the QNSE scheme in WRF when compared to measurements from CMET balloons over Svalbard as well as compared to timeseries taken from three different weather stations situated in Ny Ålesund, Verlegenhuken and Hopen. WRF was run with two different domain setups, where the first case included the timeseries from Ny Ålesund and Verlegenhuken and six profiles in the vicinity of Ny Ålesund and the second case included the timeseries from Hopen and two profiles over sea ice to the east of the Svalbard archipelago.

2 The numerical model

The Advanced Research WRF Model Version 3.3.1 was used for the numerical simulations. WRF was developed by the National Center for Atmospheric Research (NCAR) and provides multi-nested domains as well as a wide range of physical parameterisations to choose among. The equations used in the model are non-hydrostatic and fully compressible Euler equations that are integrated along terrain-following hydrostatic-pressure vertical (sigma) coordinates. For a detailed description of WRF, see Skamarock et al. (2008).

The model was run for the simulation period from 3 May 2011 00:00 UTC to 12 May 2011 00:00 UTC allowing for a spinup time of 48 hours. Three domains with a respective horizontal resolution of 9km, 3km and 1km were used, where the two inner domains both were two-way nested to their mother domain. The outer domain was centered at 78.9°N, 16.5°E (78.9°N, 19.5°E for model run 2) and included 114 x 94 gridpoints covering the whole Svalbard archipelago and a large part of the Atlantic around it. The second domain included 175 x 184 (187 x 202) gridpoints for model run 1 (model run 2) and covered the whole Svalbard archipelago and a small part of the Atlantic around it. Its position varied slightly between the two cases, depending on the position of the

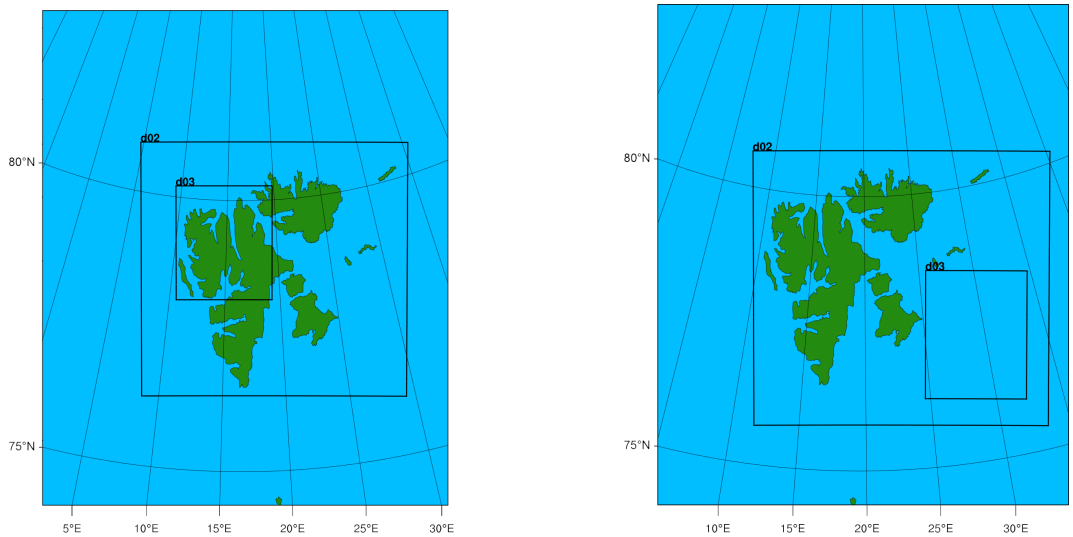

(a) Model run 1

(b) Model run 2

Figure 2.1: Domain setup for the two model runs.

innermost domain, which covered the area where the correspondent balloon profiles and timeseries were measured with 232 x 190 (253 x 202) gridpoints for model run 1 (model run 2). The domains are sketched in Figure 2.1. All three domains had a high vertical resolution with 61 terrain-following sigma levels, where the model top was set to 50hPa. The lowest 1000m included 19 model levels with the lowest full model level at 19m. According to Mayer et al. (2012b), at least 61 vertical levels are necessary to resolve ABL phenomena, such as low level jets.

Static field data, such as topography and landuse index, were provided by the US Geological Survey in a horizontal resolution of $30''$ (0.9km in north-south direction). The latitude-longitude dataset was interpolated to the stereographic grid that is used in WRF with the WRF Preprocessing System (WPS). Initial and lateral boundary conditions were taken from the ECMWF operational analysis data on a 0.125° x 0.125° horizontal resolution and on 91 vertical levels. The boundaries were updated every six hours. Running WRF can therefore be interpreted as dynamical downscaling (both in space and in time).

Due to very high wind speeds on 9 May 2011, numerical instability occurred and lead to a crashing of the model even when a comparably small time step of 30s was used. Therefore we decided to use an adaptive time step, which means that the time step was allowed to vary over the simulation period depending on the stability criteria. It could go down to 1s.

Furthermore, the following physical parameterisations were applied: For cloud microphysics the WRF single moment 3-class simple ice scheme (Dudhia, 1989; Hong et al., 2004) was used. Radiation was parameterised with the Rapid Radiative Transfer Model (RRTM) longwave scheme (Mlawer et al., 1997), and the Dudhia shortwave scheme (Dudhia, 1989). Surface fluxes were provided by the Noah Land Surface Model (LSM), a four-layer soil temperature and moisture model with snow cover prediction (Chen and Dudhia, 2001). In the first and second domain, the Kain-Fritsch cumulus scheme (Kain, 2004) was applied in addition, whereas in the third domain, cumulus convection was neglected.

Sensitivity tests were made with three different boundary layer parameterisation schemes: The Yonsei University (YSU) scheme, the Mellor-Yamada-Janjic (MYJ) scheme and the Quasi-Normal Scale Elimination (QNSE) scheme. The YSU scheme (Hong et al., 2006) is a non-local first order closure scheme that uses a countergradient term in the eddy diffusion equation. It is successor to the Medium Range Forecast (MRF) scheme, which was used in the WRF predecessor Mesoscale Meteorology Model 5 (MM5), and is the default ABL scheme in WRF. The MYJ scheme (Janjic, 1990, 1996, 2002) uses the local 1.5 order (level 2.5) closure Mellor-Yamada Model (Mellor and Yamada, 1982), where the eddy diffusion coefficient is determined from the prognostically calculated turbulent kinetic energy (TKE). According to Mellor and Yamada (1982), it is an ap-

propriate scheme for stable to slightly unstable flows, while errors might occur in the free convection limit. The QNSE scheme (Sukoriansky et al., 2006) is, as the MYJ scheme, a local 1.5 order closure scheme. In contrast to the MYJ scheme, it includes scale dependence by using only partial averaging instead of scale independent Reynolds averaging, and is therefore able to take into account the spatial anisotropy of turbulent flows. It is especially suited for the stable ABL.

2.1 Sea Ice

Sea ice is an important factor influencing the latent and sensible heat fluxes between ocean and atmosphere as well as the radiation balance of the surface, thereby affecting the temperature and humidity profiles over land and sea. Thus it is important that the sea ice sheet is correctly implemented into WRF. In this study, sea ice and sea surface temperature (SST) were taken directly from the ECMWF data at the time the simulation started and remained fixed during the whole simulation period. Fractional sea ice was not included, meaning that a grid point was either not or fully covered by sea ice. To find out whether this approach was a reasonable way to implement sea ice, the ECMWF data was compared to a satellite picture from 5 May 2011 (Figure 2.2). In fact, the two sea ice sheets look very similar, only to the east of the southern edge of Svalbard, sea ice extends slightly too far south in the ECMWF data compared to the satellite picture. In addition, there are some holes in the sea ice sheet to the east of Svalbard in the satellite picture, which cannot be seen in the ECMWF data. However, since these smaller deficiencies do not directly affect the area where the balloon profiles were made, we left the sea ice from the ECMWF data unmodified for a start.

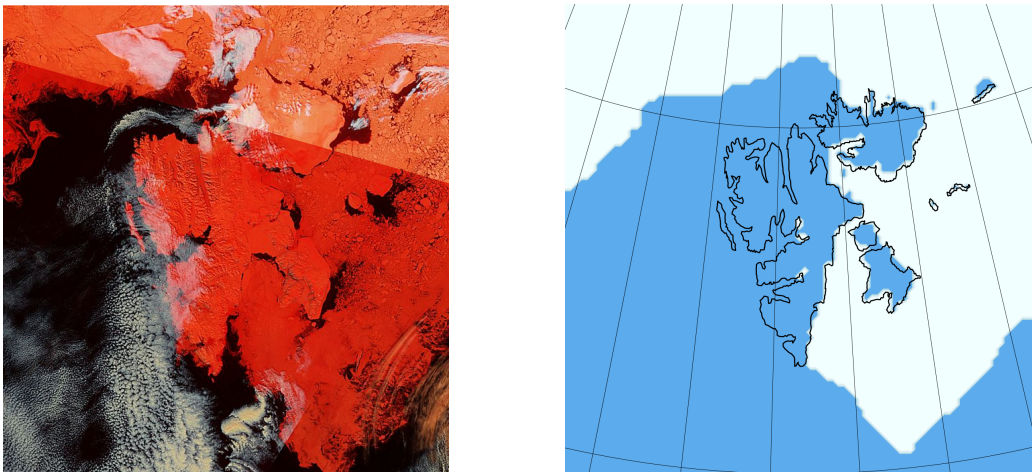

Figure 2.2: Satellite picture of Svalbard on 5 May 2011 (left) and the sea ice flag implemented into WRF (right).

3 The balloon flights

Figure 3.1 and 3.2 show the balloon flights of the May 2011 campaign. The balloons were launched from the research station of the Alfred Wegener Institute and the Polar Institute Paul Emile Victor (together AWIPEV) in Ny Ålesund. The total observational period lasted from 5 May 2011 to 12 May 2011. Balloons 1 and 2 did not fly very far and included only one vertical sounding each. Balloon 3 flew far north but stayed below 600m after leaving the coastal area of the Spitsbergen island, thus only the vertical sounding (up and down) at the very beginning of the flight could be used for this study. Balloon 4's flight went far to the east and included a vertical sounding at the beginning, which was used for comparison with the first model run, and two closely spaced (up and down) soundings at the end that were used for comparison with the second model run. Balloon 5 flew first northwards and then eastwards along the coast and measured a series of 18 consecutive profiles in the beginning of the flight. It was the first free balloon to measure such a long sequence of profiles during transport. The flight is described in detail by Voss et al. (2012). For the comparison with the first model run, the first and the last profile of the series were chosen.

In total, we selected 6 profiles for the first model run and 2 profiles for the second model run to compare with WRF. The ranges of each profile are indicated by a gray band in Figure 3.2. In case of an up and down sounding, the values of the two profiles were averaged over height. Furthermore, the profiles were interpolated to 50m height intervals to obtain a smoother structure. The respective time frames in WRF that most closely matched the average time during which the corresponding balloon profile was taken, i.e., the full hour that approximately lay in the middle of the balloon profile, were selected for the comparison. The longitude and latitude of the WRF profile cor-

Date (UTC)	Pressure	2m temp.	Rel. humidity	10m wind
Model run 1				
05 May 2011 18:00	1023.4 hPa	-2.1 °C	68.1 %	1.2 m/s
06 May 2011 14:00	1027.7 hPa	1.2 °C	71.0 %	2.9 m/s
06 May 2011 22:00	1025.7 hPa	2.1 °C	61.3 %	4.8 m/s
07 May 2011 15:00	1018.2 hPa	0.3 °C	83.6 %	2.8 m/s
11 May 2011 03:00	1033.3 hPa	-8.2 °C	51.7 %	0.8 m/s
11 May 2011 12:00	1033.8 hPa	-4.7 °C	53.0 %	1.0 m/s
Model run 2				
08 May 2011 09:00	1008.9 hPa	-1.8 °C	89.0 %	4.9 m/s
08 May 2011 11:00	1009.1 hPa	-2.8 °C	86.6 %	3.9 m/s

Table 3.1: Meteorological data from Ny Ålesund at the times of the balloon profiles.

responded to the grid point that lay closest to the location of the balloon when it was at its maximum height during the respective profile (see Figure 3.3 for the locations for model run 1 and Figure 3.1 for model run 2). The times are listed in Table 3.1 together with the most important meteorological data from Ny Ålesund at the given time. In addition, the lines in Figure 4.1 indicate the times when the WRF profiles were taken.

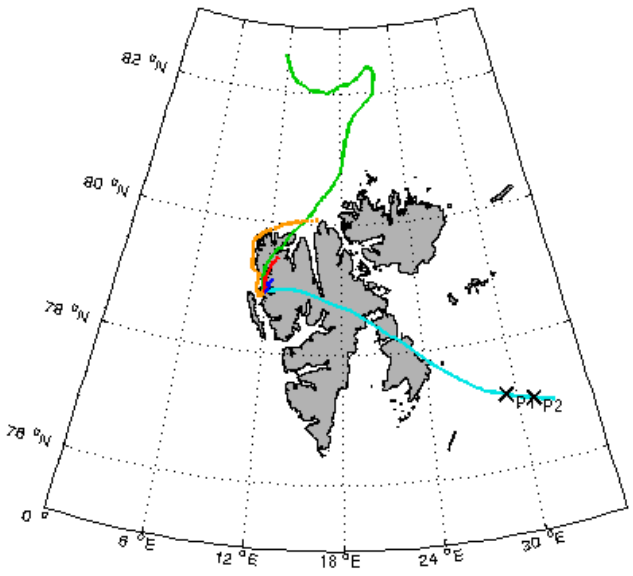

Figure 3.1: Trajectories of the CMET balloons (lat vs. lon) and locations of the profiles for model run 2.

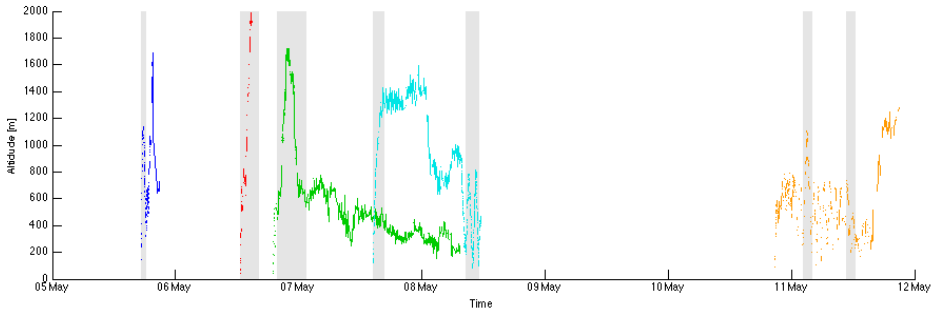

Figure 3.2: Trajectories of the CMET balloons (altitude vs. time). The grey bands indicate the ranges of the profiles chosen for the comparison.

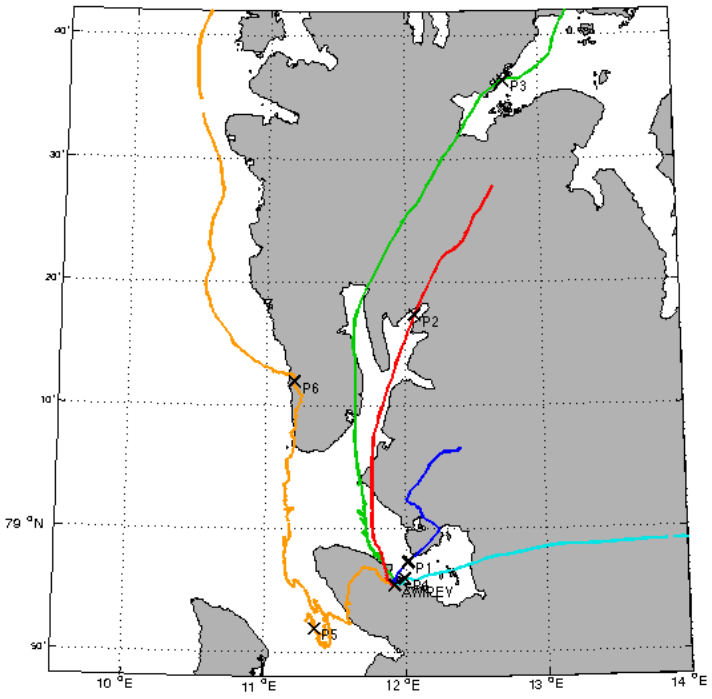

Figure 3.3: Locations of the profiles for model run 1.

3.1 Comparison with radiosoundings

To verify that the CMET balloons measured the meteorological parameters correctly, the profiles that were taken close to Ny Ålesund, i.e., the ones used for model run 1, were compared with radiosoundings from the AWIPEV station in Ny Ålesund, where a radiosonde was launched each day at 11:00 UTC (Figure 3.4 to 3.7). Note that the CMET balloon profiles and the radiosoundings were not measured exactly at the same time or location, which can explain the slight differences especially in the shape of the profiles. Figure 3.3 shows the locations where the balloon profiles were taken together with the location of the AWIPEV station. For the comparison, the two radiosonde profiles that were closest in time to the balloon profile, i.e. the one before and the one after, were chosen, where the first radiosounding is depicted in darker blue and the second in lighter blue (Figure 3.4 to 3.7). The difference in time to the profile that lies closest is noted as 'Diff'. A positive number indicates that the balloon sounding came after the closest radiosounding, meaning that the balloon profile lies closer in time to the blue profile, and vice versa.

For wind speed, balloon profiles 1, 5 and 6 lie well between the two radiosonde profiles. Balloon 4 shows a slightly lower wind speed than the radiosondes, but otherwise the profile looks similar to the blue profile, showing higher wind speeds at the upper levels than at the lower levels. Balloon 2 and 3 measured a higher wind speed than the radiosondes, especially a higher low level jet at around 1200m. This can most probably be explained by the different locations, both profile 2 and 3 were measured far north of the station where the radiosonde was launched. In addition there is a large temporal difference between balloon profile 3 and the radiosoundings.

For potential temperature, the balloon profiles agree very well with the radiosonde profiles. The slope and the magnitude of all the profiles accord almost perfectly to the radiosonde profiles, especially the inversion in profile 2 and 3 is well captured by the balloons. Balloon 2 measured a slightly higher temperature than the radiosonde in particular at high levels, which is most probably due to the difference in daytime.

The relative humidity profiles show a similar structure but generally lower values for the balloons than for the radiosondes, except for balloon 5, where the profiles (5 and 6) lie in between the two radiosonde profiles. Relative humidity can vary highly spatially as well as temporally, and is therefore difficult to compare between different time and locations (e.g., clouds may move, appear or disappear). Nevertheless, the slope, vertical structure and general magnitude of the profiles measured by the balloons show a reasonable picture.

Wind direction might be equally difficult to compare, in particular between different locations, due to different topography, which influences wind direction especially at low levels. In addition, there was high temporal variation in large scale wind direction during the period (see Section 4.1), which can also be seen in the difference between the radiosonde profiles. For constant wind direction, i.e., where the two radiosonde profiles coincide, the wind direction measured by the balloons does not substantially differ from the radiosondes' wind direction.

Hence, we assume that the balloons measured the meteorological parameters correctly. The differences in some of the profiles (e.g., relative humidity) however imply that we cannot say so with absolute certainty.

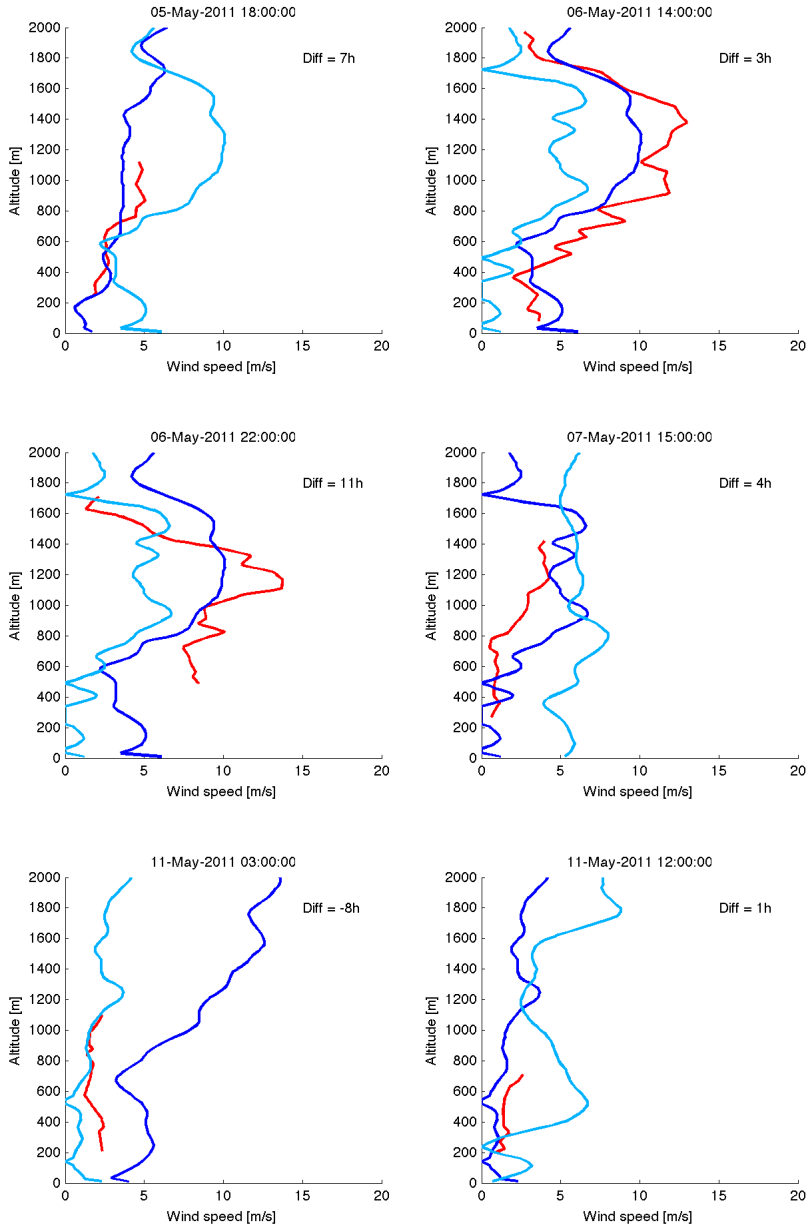

Figure 3.4: Radiosoundings and CMET balloon profiles of wind speed. The radiosounding taken before the balloon profile is depicted in dark blue, the one after in light blue. 'Diff' indicates the temporal difference between the balloon profile and the closest radiosounding.

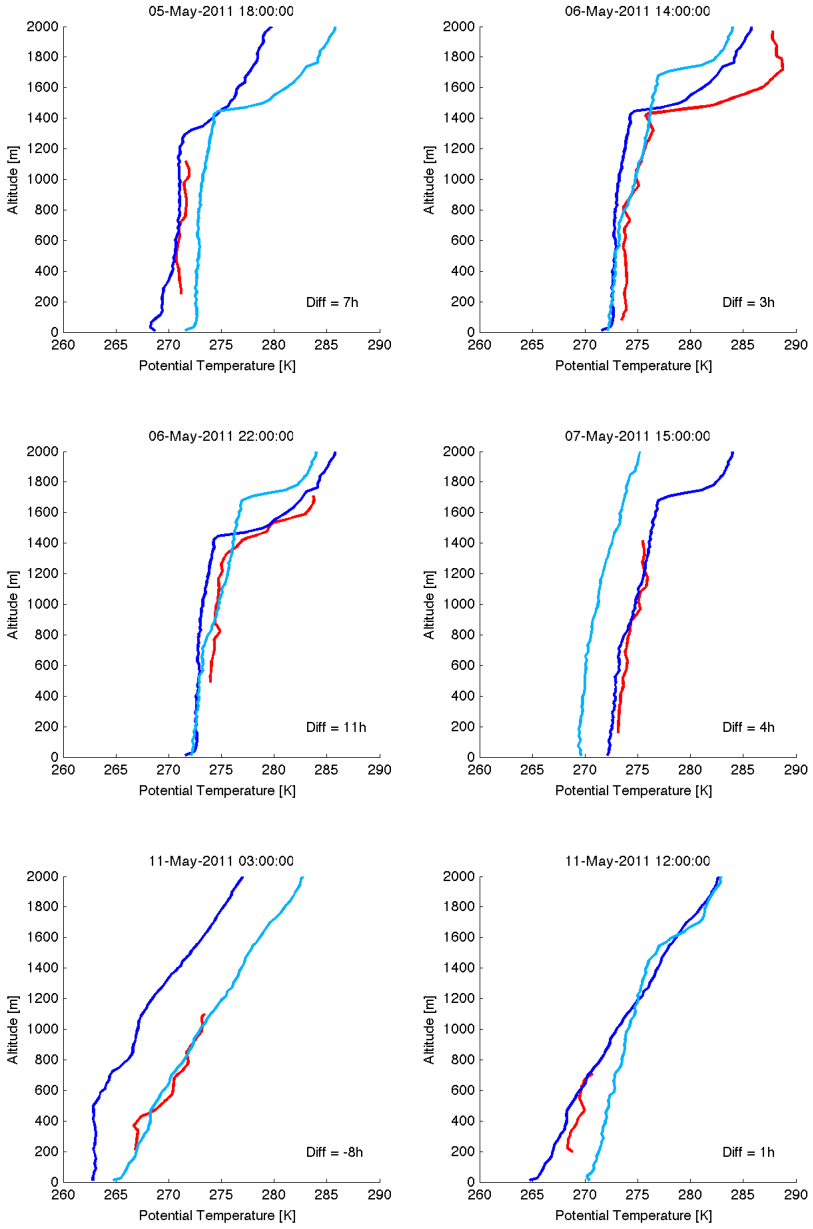

Figure 3.5: Radiosoundings and CMET balloon profiles of potential temperature. Colours as in Figure 3.4

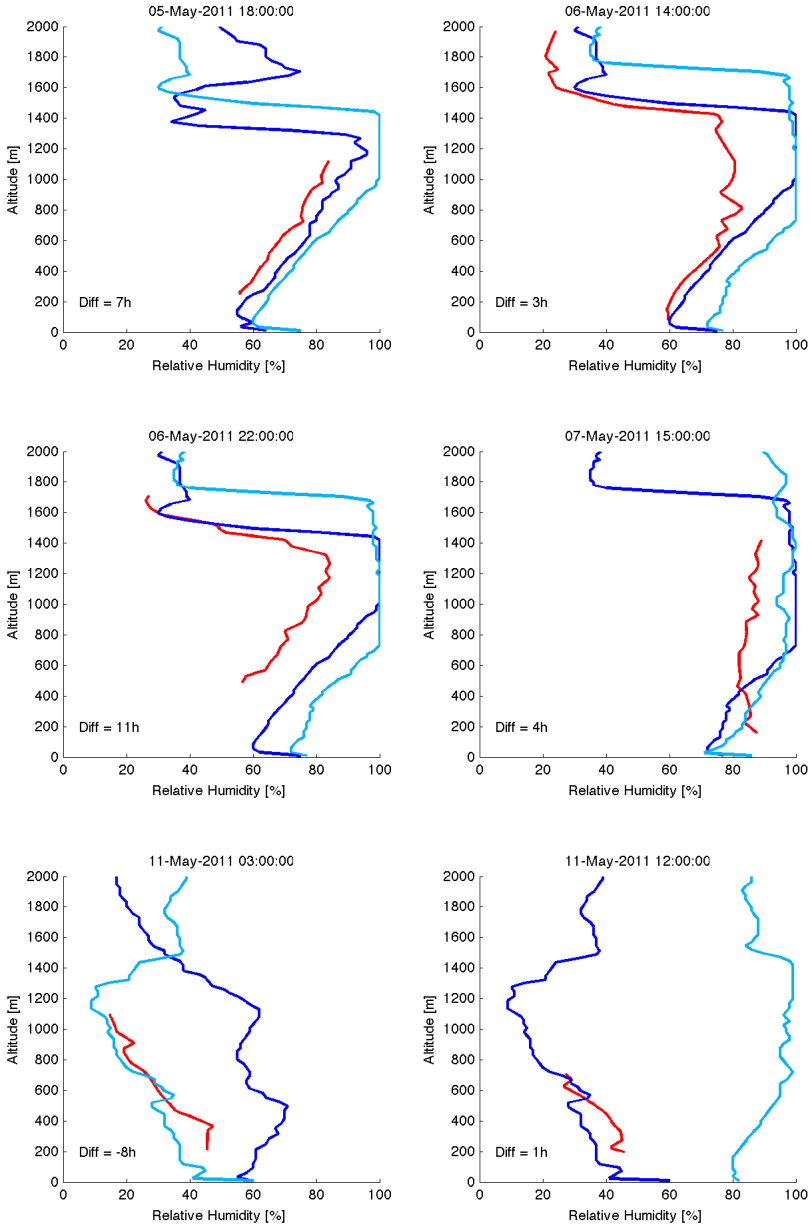

Figure 3.6: Radiosoundings and CMET balloon profiles of relative humidity. Colours as in Figure 3.4

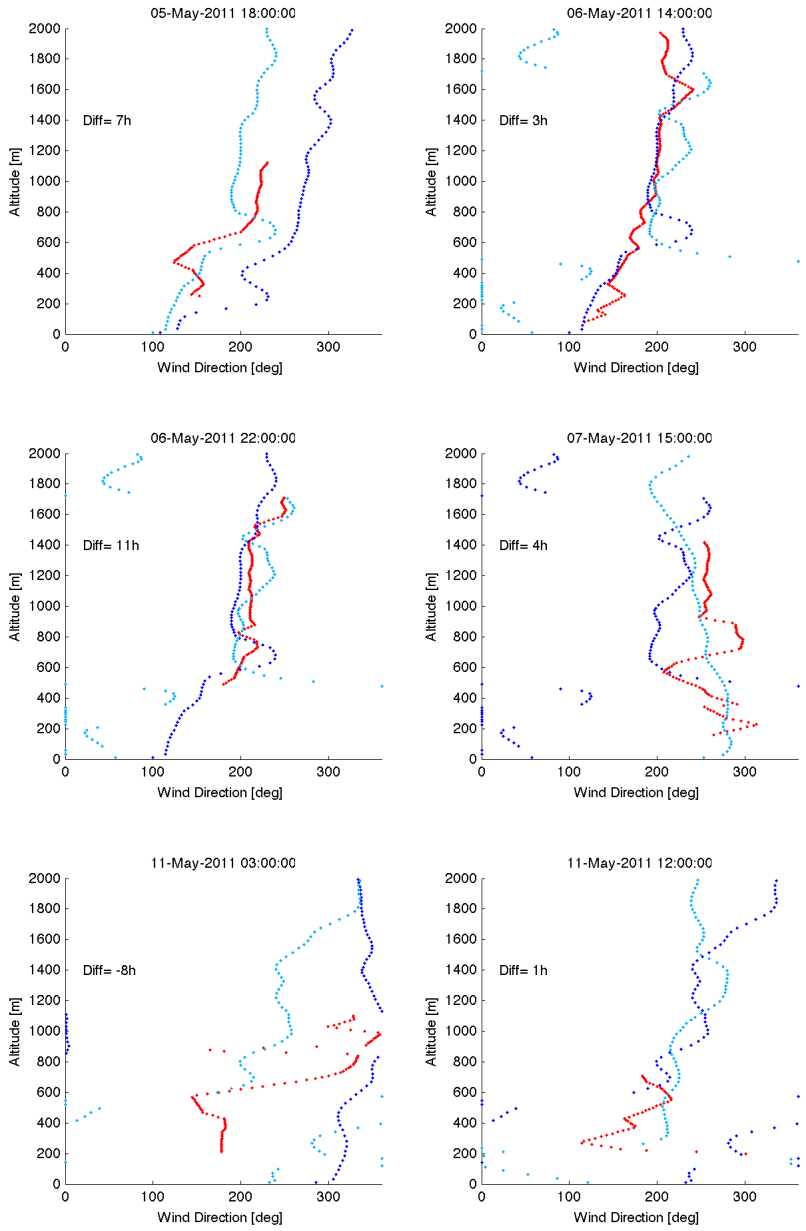

Figure 3.7: Radiosoundings and CMET balloon profiles of wind direction. Colours as in Figure 3.4

4 Results

4.1 The synoptical situation

The period of 1-12 May 2011 is characterised by rapidly changing meteorological conditions. In the very beginning, a small low pressure system is developing north of the Svalbard archipelago, moving gradually eastwards. This leads to northerly winds carrying cold air from the north towards Svalbard and Ny Ålesund. Weather data from the AWIPEV station in Ny Ålesund (Figure 4.1) show that temperature starts to sink on 2 May until it reaches a first minimum of -9.4°C in the night to 5 May. After that, the main wind direction changes from north to south in not much more than one day. Hence, temperature in Ny Ålesund increases and reaches 2.9°C on 6 May. The wind direction then becomes more westerly and pressure decreases as a high pressure system that had developed in the south east moves even further eastwards and away from Svalbard. On 8 May two low pressure systems develop north and east of the Svalbard archipelago. They merge only a few hours later and build a strong low to the north east of Svalbard, which intensifies and, combined with an approaching high pressure system from the west, leads to a strong pressure gradient over the island and hence high wind speeds on 8 and 9 May. At the AWIPEV station the maximum wind speed registered is 17.3m/s on 9 May around noon. Due to the strong northerly winds, temperature in Ny Ålesund falls below -10°C on 10 and 11 May. Later, the high pressure system coming from the west banishes the low pressure system from over Svalbard and calms the situation down. Pressure and temperature increase again and wind speeds decrease.

Figure 4.2 shows the evolution of the synoptical situation in WRF (model run 1 with the YSU scheme) compared to the ECMWF operational analysis data. The wind field is interpolated to 10m in WRF, while taken from the lowest model level in the ECMWF data. WRF manages to reproduce the wind field and the sea level pressure evolution very well, especially the high winds and strong pressure gradient on 9 May are perfectly reproduced. However, the model generally underestimates surface temperature over land and over sea ice. With increasing simulation time, surface temperature over sea ice decreases compared to the ECMWF data and the border between the sea ice flag and the open sea becomes more visible. This might particularly affect the profiles taken over sea ice to the east of Svalbard (Section 4.3). Temperature over the open sea is reasonably reproduced throughout the whole simulation time. It must be mentioned that neither the ECMWF operational analysis data necessarily represent reality.

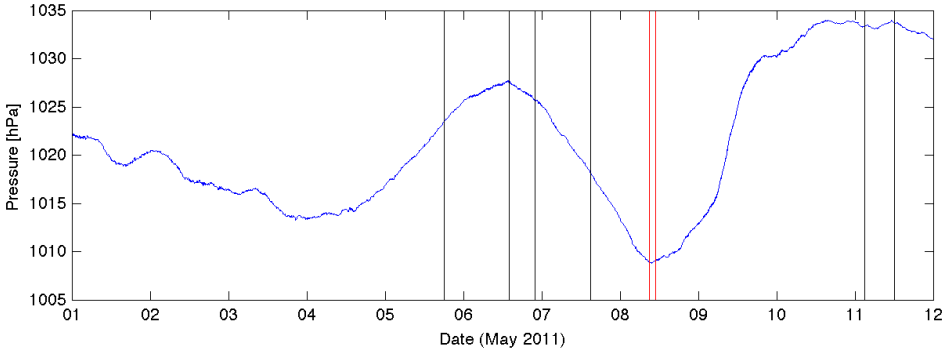

(a) Pressure

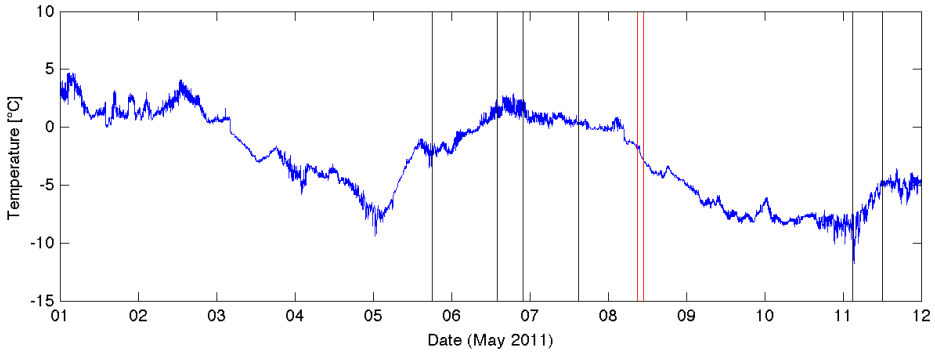

(b) Temperature at 2m

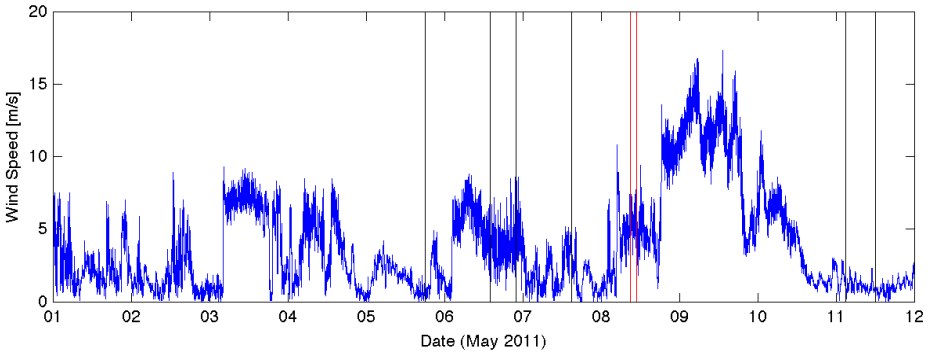

(c) Maximum wind speed for a minute at 10m

Figure 4.1: Meteorological data from the AWIPEV station in Ny Ålesund. The lines indicate the times of the profiles in WRF (black: model run 1, red: model run 2).

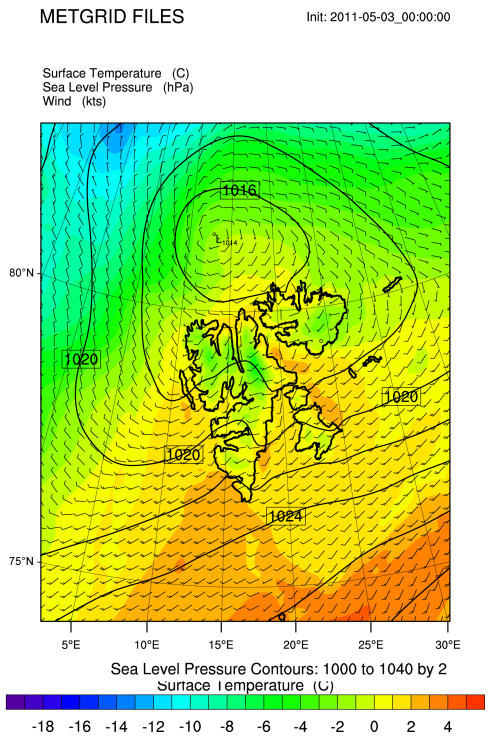
METGRID FILES
Init: 2011-05-03_00:00:00
Surface Temperature (C)
Sea Level Pressure (hPa)
Wind (kts)
80°N
75°N
5°E
10°E
15°E
20°E
25°E
30°E
1016
1020
1024
Sea Level Pressure Contours: 1000 to 1040 by 2
Surface Temperature (C)
-18 -16 -14 -12 -10 -8 -6 -4 -2 0 2 4

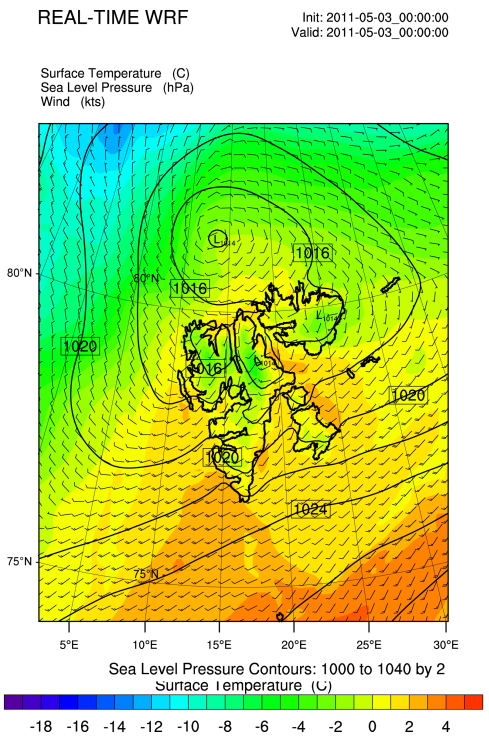
REAL-TIME WRF
Init: 2011-05-03_00:00:00
Valid: 2011-05-03_00:00:00
Surface Temperature (C)
Sea Level Pressure (hPa)
Wind (kts)
80°N
75°N
5°E
10°E
15°E
20°E
25°E
30°E
1016
1020
1024
Sea Level Pressure Contours: 1000 to 1040 by 2
Surface Temperature (C)
-18 -16 -14 -12 -10 -8 -6 -4 -2 0 2 4

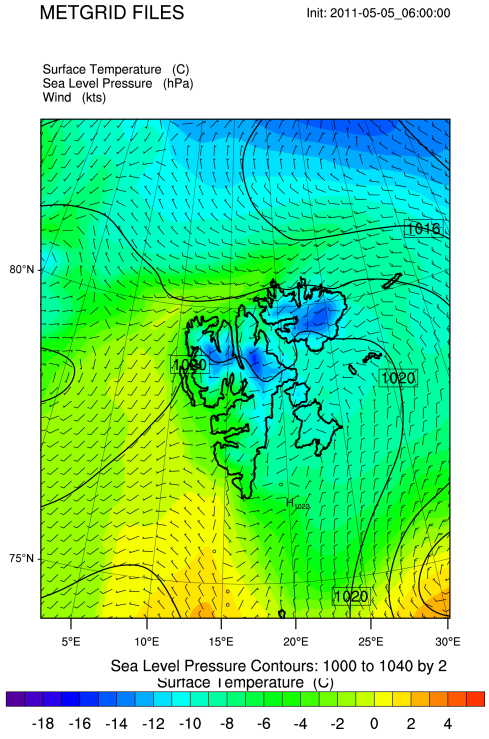
METGRID FILES
Init: 2011-05-05_06:00:00
Surface Temperature (C)
Sea Level Pressure (hPa)
Wind (kts)
80°N
75°N
5°E
10°E
15°E
20°E
25°E
30°E
1016
1020
Sea Level Pressure Contours: 1000 to 1040 by 2
Surface Temperature (C)
-18 -16 -14 -12 -10 -8 -6 -4 -2 0 2 4

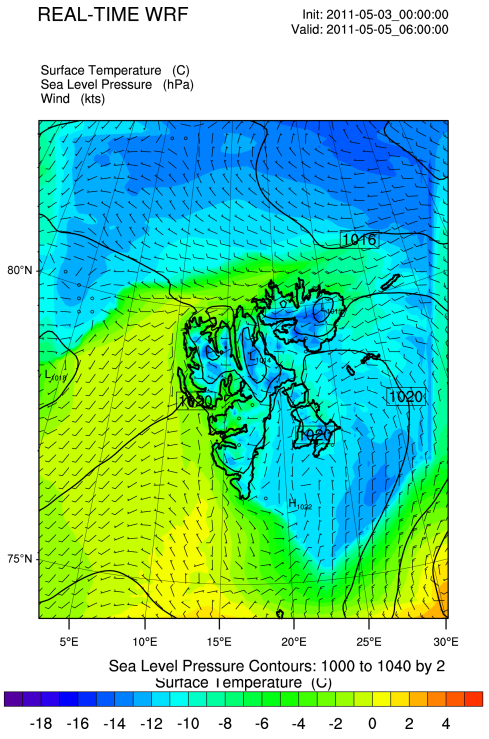
REAL-TIME WRF
Init: 2011-05-03_00:00:00
Valid: 2011-05-05_06:00:00
Surface Temperature (C)
Sea Level Pressure (hPa)
Wind (kts)
80°N
75°N
5°E
10°E
15°E
20°E
25°E
30°E
1016
1020
Sea Level Pressure Contours: 1000 to 1040 by 2
Surface Temperature (C)
-18 -16 -14 -12 -10 -8 -6 -4 -2 0 2 4

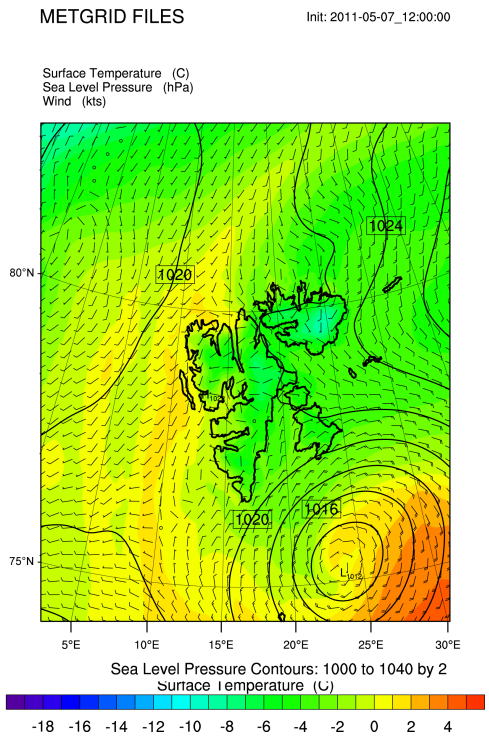
METGRID FILES
Init: 2011-05-07_12:00:00
Surface Temperature (C)
Sea Level Pressure (hPa)
Wind (kts)
80°N
75°N
5°E
10°E
15°E
20°E
25°E
30°E
1024
1020
1016
Sea Level Pressure Contours: 1000 to 1040 by 2
Surface Temperature (C)
-18 -16 -14 -12 -10 -8 -6 -4 -2 0 2 4

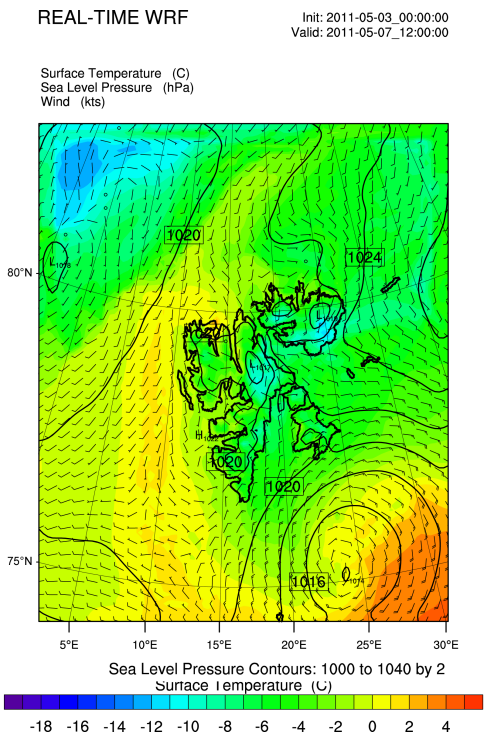
REAL-TIME WRF
Init: 2011-05-03_00:00:00
Valid: 2011-05-07_12:00:00
Surface Temperature (C)
Sea Level Pressure (hPa)
Wind (kts)
80°N
75°N
5°E
10°E
15°E
20°E
25°E
30°E
1020
1024
1016
Sea Level Pressure Contours: 1000 to 1040 by 2
Surface Temperature (C)
-18 -16 -14 -12 -10 -8 -6 -4 -2 0 2 4

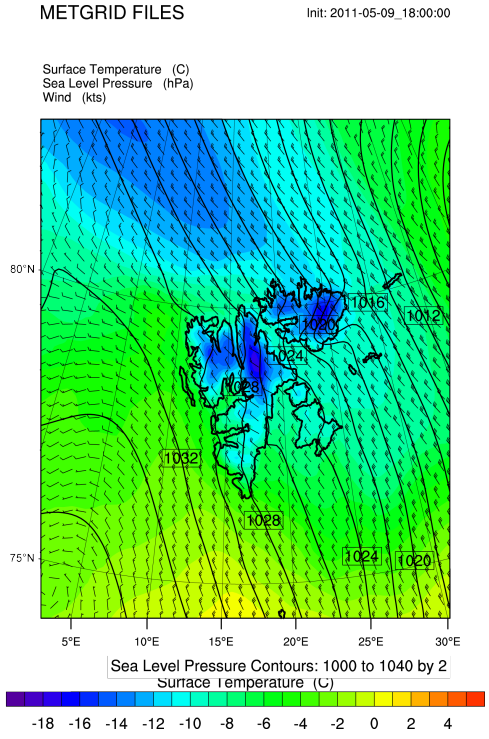
METGRID FILES
Init: 2011-05-09_18:00:00
Surface Temperature (C)
Sea Level Pressure (hPa)
Wind (kts)
80°N
75°N
5°E
10°E
15°E
20°E
25°E
30°E
1016
1012
1020
1024
1028
1032
Sea Level Pressure Contours: 1000 to 1040 by 2
Surface Temperature (C)
-18 -16 -14 -12 -10 -8 -6 -4 -2 0 2 4

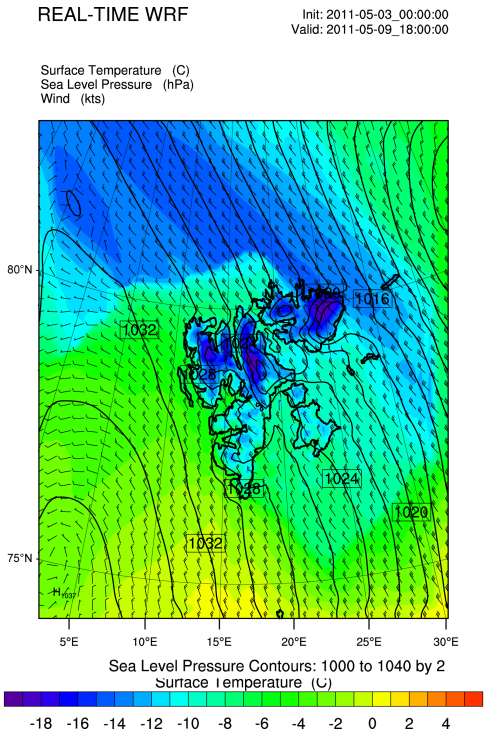
REAL-TIME WRF
Init: 2011-05-03_00:00:00
Valid: 2011-05-09_18:00:00
Surface Temperature (C)
Sea Level Pressure (hPa)
Wind (kts)
80°N
75°N
5°E
10°E
15°E
20°E
25°E
30°E
1016
1032
1028
1024
1020
Sea Level Pressure Contours: 1000 to 1040 by 2
Surface Temperature (C)
-18 -16 -14 -12 -10 -8 -6 -4 -2 0 2 4

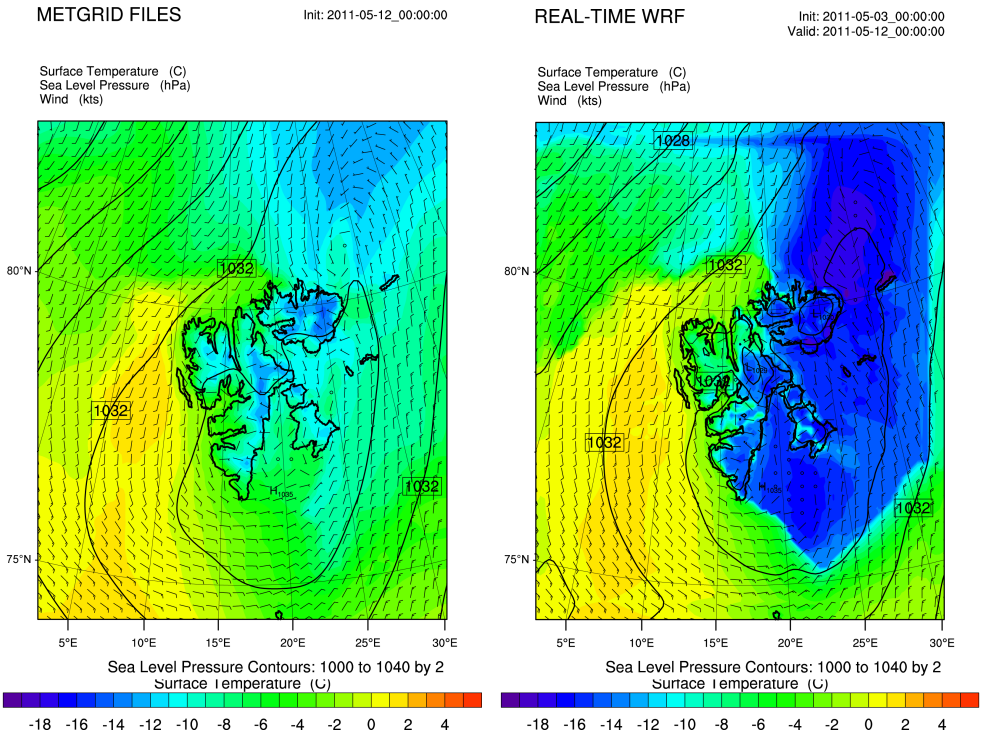

Figure 4.2: Evolution of surface temperature, sea level pressure and wind field in the ECMWF data (left) and WRF (right).

4.2 Model run 1: Coastal area

In the first model run, the innermost domain covered the north eastern part of the Spitsbergen island, including the locations of the weather stations in Ny Ålesund and Verlegenhuken and six profiles measured by the CMET balloons in the coastal area of the island (Figure 2.1a). The locations of the balloon soundings are marked in Figure 3.3. Figures 4.3 to 4.7 show the evaluation of the WRF model with the three different boundary layer schemes. The grey band represents a range of 25 profiles of the YSU scheme on a 4km x 4km square that is centered at the grid point closest to the balloon profile. It illustrates the horizontal variability in the model output. In table 4.1 the mean absolute error and the mean bias error for each scheme and profile are listed.

WRF captures the profiles with weak winds (profile 1, 4, 5, 6) very well, but tends to overestimate the wind speeds in case of stronger winds (profile 2, 3), especially at low levels. The observations show a weak low level jet with a wind speed maximum at around 1200m and lower wind speeds above and below. WRF in contrast has the highest wind speeds below 1000m. This leads to a large mean absolute error in profile 2 and 3. The

different ABL schemes are not strongly differing from each other, it is however the YSU scheme that has the least mean absolute error and absolute bias for the total wind speed.

The potential temperature profiles are well reproduced in the lower levels, except for profile 6, where WRF (especially the MYJ and the QNSE scheme) underestimates temperature by around 2K. In profile 2 and 3, an inversion can be seen in the observations above 1300m, which WRF does not capture. Although it shows an increase in the gradient, the location and the strength of the inversion are not correct. It lies too high in profile 2, and too low in profile 3. The three ABL schemes are in strong agreement among themselves on both magnitude and slope of the profile. Again, the YSU scheme has the least mean absolute error as well as the least (absolute) bias.

Relative humidity is overestimated by WRF in the low levels (especially profile 1, 6) and underestimated in higher levels (profile 2, 3). In profile 1 to 4, WRF shows a much shallower ABL than the balloons (defining the height where relative humidity begins to decrease as the upper level of the ABL). The two profiles measured by balloon 5 (i.e., profile 5 and 6) look very similar with relative humidity being around 40% at 200m and decreasing to 20% at 800m. WRF represents the first of the two profiles appropriately but in contrast to reality shows a strong increase in relative humidity during the nine hours that lie between the two profiles, most pronounced for the QNSE scheme. This might be due to uncorrect representation of moist air advection in the model. Except for the first profile, the YSU scheme is the one that lies closest to the observations. It also has the lowest mean absolute error and, apart from profile 1 and 4, the lowest bias.

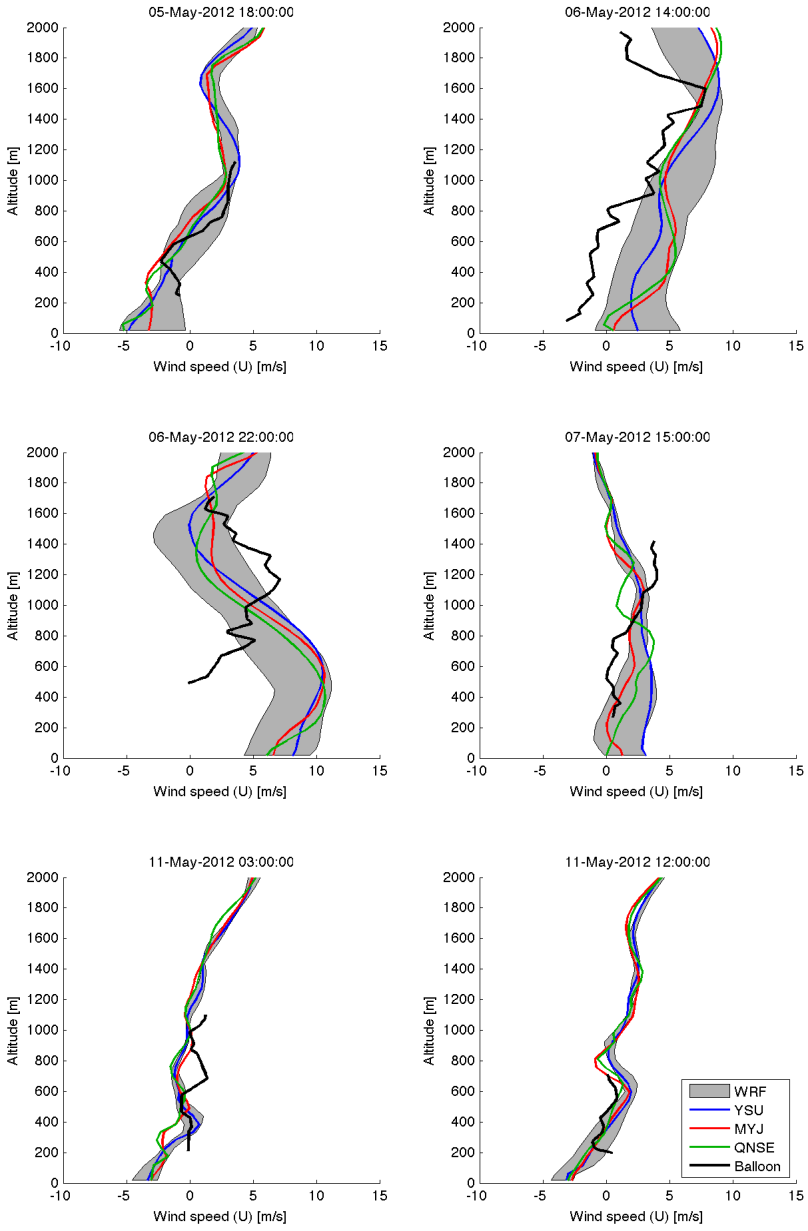

Figure 4.3: Observed and modelled wind (u) profiles. The profiles modelled by the three ABL schemes are in colour, the observed profile is in black. The grey band represents a range of 25 profiles of the YSU scheme on a 4km x 4km square centered at the grid point closest to the observation site.

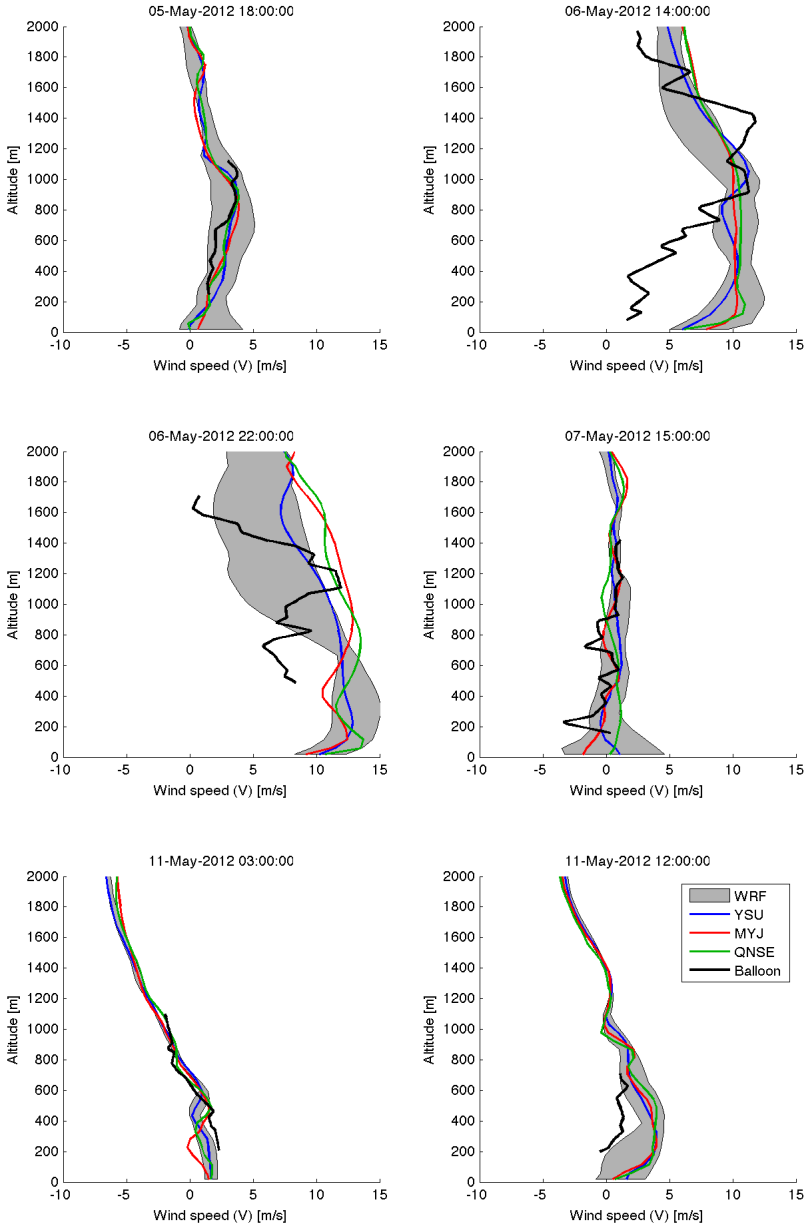

Figure 4.4: Observed and modelled wind (v) profiles. Grey band and colours as in Figure 4.3.

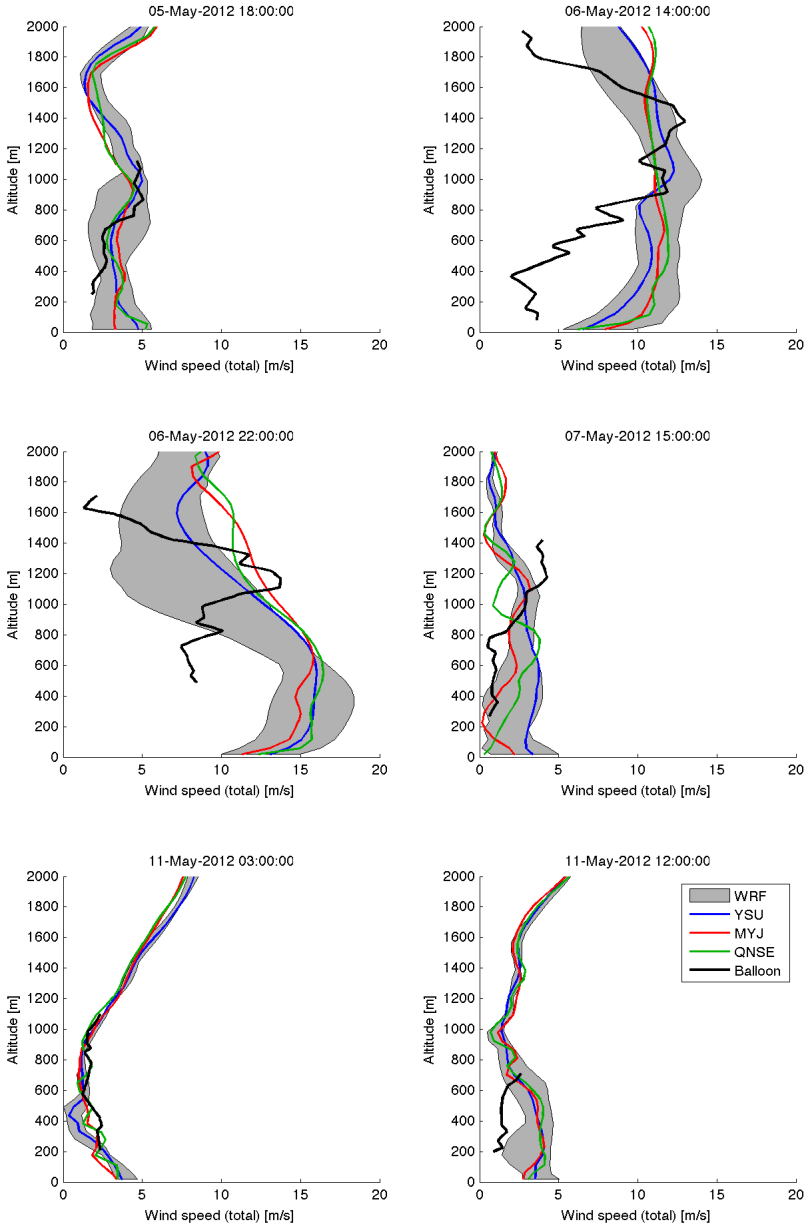

Figure 4.5: Observed and modelled wind (total) profiles. Grey band and colours as in Figure 4.3.

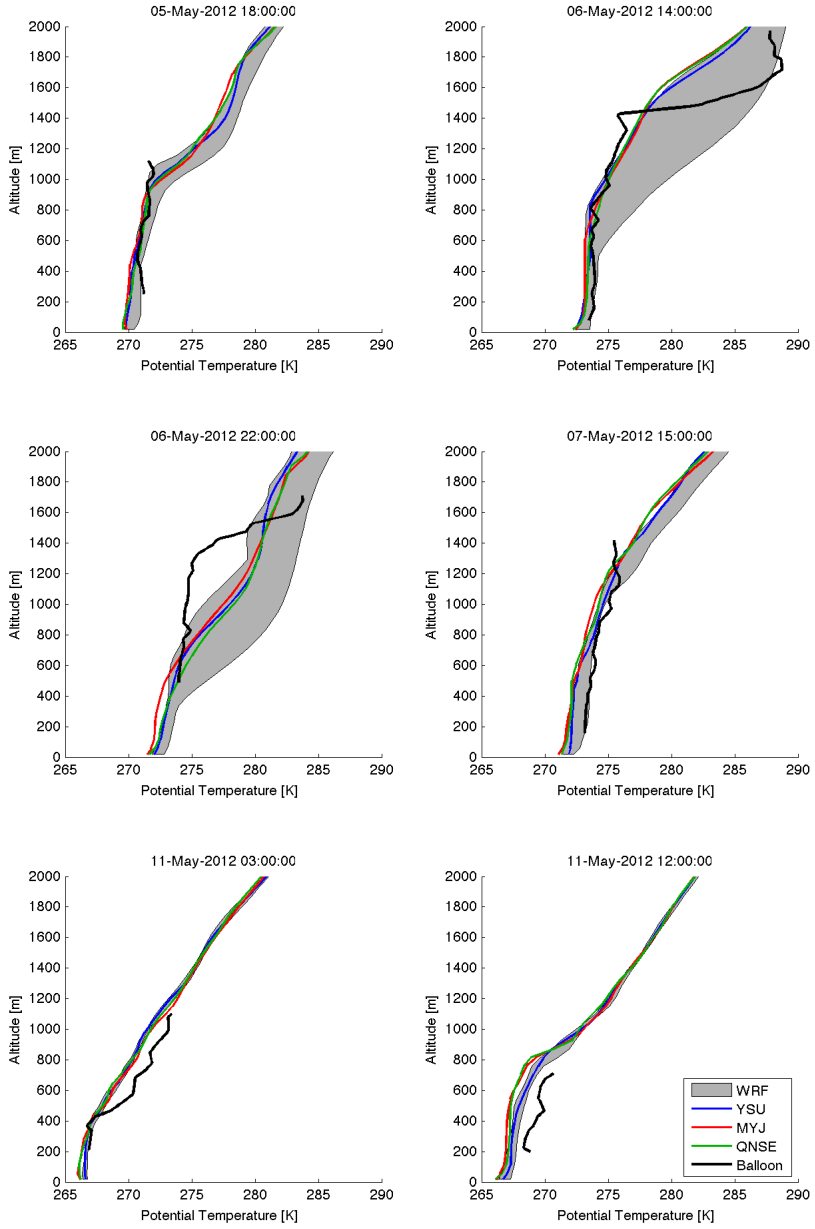

Figure 4.6: Observed and modelled potential temperature profiles. Grey band and colours as in Figure 4.3.

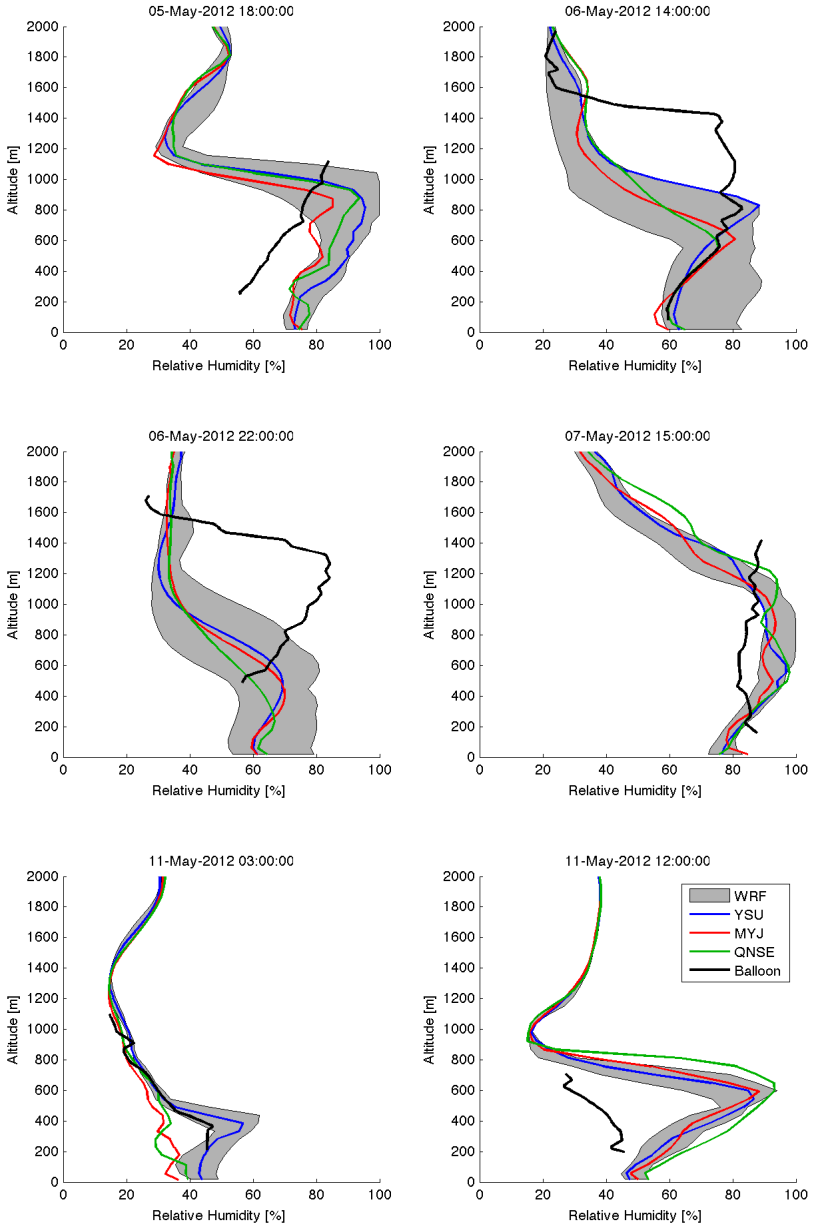

Figure 4.7: Observed and modelled relative humidity profiles. Grey band and colours as in Figure 4.3.

	Mean abs. error			Mean bias error		
Wind (u)	YSU	MYJ	QNSE	YSU	MYJ	QNSE
Profile 1	0.7259	1.1554	1.0781	-0.2765	-1.1554	-0.8289
Profile 2	3.3675	3.7137	3.5772	3.3675	3.6869	3.5733
Profile 3	4.4004	3.9208	4.0474	1.1609	1.2301	0.4173
Profile 4	1.9725	1.1385	2.0199	1.0097	-0.1212	0.2799
Profile 5	1.0082	1.1418	1.3047	-0.8214	-1.0042	-1.2687
Profile 6	0.8185	0.5377	0.4399	0.7788	0.5138	0.3525
Average	**2.0488**	**1.9347**	**2.0779**	**0.8698**	**0.5250**	**0.4209**
Wind (v)						
Profile 1	0.7111	0.6796	0.5473	0.4511	0.3213	0.2404
Profile 2	3.0068	3.4173	3.5452	2.1320	2.4497	2.6697
Profile 3	3.4304	4.5488	4.7746	2.9552	4.5488	4.7158
Profile 4	0.7424	0.5027	1.1261	0.5635	0.3384	0.4858
Profile 5	0.6889	0.6587	0.5047	-0.2154	-0.3005	-0.1806
Profile 6	2.0594	2.1563	2.4129	2.0594	2.1563	2.4129
Average	**1.7732**	**1.9939**	**2.1518**	**1.3243**	**1.5857**	**1.7240**
Wind (total)						
Profile 1	0.5609	0.9381	0.7687	0.2837	0.3234	0.0963
Profile 2	3.4914	4.0992	4.2508	3.2142	3.4867	3.6976
Profile 3	4.3992	4.9400	5.0845	3.2411	4.6842	4.5081
Profile 4	1.8861	1.0433	1.9871	0.9089	-0.2294	0.1691
Profile 5	0.5465	0.3547	0.2920	-0.4501	-0.2578	-0.1778
Profile 6	1.8598	1.9355	2.0246	1.7766	1.7634	1.9578
Average	**2.1240**	**2.2184**	**2.4013**	**1.4957**	**1.6284**	**1.7085**
Pot. temp.						
Profile 1	0.5121	0.7127	0.4815	-0.0576	-0.1037	0.0872
Profile 2	1.6233	1.8864	1.7537	-1.2986	-1.4617	-1.3859
Profile 3	2.3796	2.2054	2.5422	1.8728	1.6729	2.1943
Profile 4	0.7460	1.0867	1.0296	-0.5103	-0.8620	-0.8149
Profile 5	1.0770	0.9397	1.0513	-1.0571	-0.9364	-1.0384
Profile 6	1.3554	2.0513	1.9328	-1.3554	-2.0513	-1.9328
Average	**1.2822**	**1.4804**	**1.4652**	**-0.4010**	**-0.6237**	**-0.4817**
Rel. humidity						
Profile 1	20.8973	15.3314	17.0006	13.7883	1.7953	8.9100
Profile 2	12.3779	16.6247	14.9303	-9.1915	-13.1670	-12.2225
Profile 3	27.2586	26.8620	27.8343	-24.1392	-24.5274	-26.5595
Profile 4	7.0112	7.8416	8.1084	2.6060	0.5462	4.7798
Profile 5	2.9870	5.2645	4.7463	2.8050	-4.8741	-3.9295
Profile 6	34.9671	35.5742	46.9129	34.9671	35.5742	46.9129
Average	**17.5832**	**17.9164**	**19.9221**	**3.4726**	**-0.7755**	**2.9819**

Table 4.1: Mean absolute error and mean bias error for the three boundary layer schemes in model run 1.

4.3 Model run 2: Sea ice

In the second model run, the innermost domain lay south east of Svalbard and covered the part over sea ice, where the fourth balloon measured two profiles, and the island Hopen, which is however not fully resolved in WRF (Figure 2.1b). The locations of the balloon soundings are marked in Figure 3.1. Figures 4.8 to 4.12 show the observed and modelled profiles for this case. Table 4.2 contains the mean absolute error and the mean bias error for each scheme and profile.

All schemes tend to overestimate wind speed, especially at the low levels, and underestimate potential temperature and relative humidity. The u component of the wind is quite correctly reproduced in the upper levels, but too high in the lower levels. The v component is overestimated over the whole height of the profile. Nevertheless the slope of the curve corresponds approximately to the observations. For total wind speed, the YSU scheme has the least bias and the least mean absolute error, although the QNSE scheme is better considering the u component.

Potential temperature is underestimated by around 2.5K in all schemes. The largest difference between the observations and the model is found at the low levels, where it reaches up to 4K. With increasing height the curves converge and only a small difference remains at the highest level. This corresponds well to the results from Section 4.1, which showed that WRF yielded too low temperatures over the sea ice flag when compared to the ECMWF data. The negative bias of surface temperature over sea ice and hence the errors in slope and magnitude of the temperature profile might indicate that there was too much sea ice in the model set up. Since fractional sea ice was not included in the model run, each grid cell was either fully covered by sea ice or not covered at all. Hence, in WRF, the according area was completely covered with sea ice, where in reality there might have been patches of open water, which would then have lead to higher temperatures above the surface. Surface temperature was even more underestimated by the MYJ and the QNSE scheme than by the YSU scheme, which was used for the comparison with the ECMWF data in Section 4.1. Nevertheless, the MYJ scheme shows the least error considering all the levels.

The relative humidity profiles are very well reproduced by the YSU scheme, in particular profile 7. It only slightly underestimates the magnitude, while the other two schemes show a high bias as well as errors in the structure of the profile. YSU also has the least mean absolute error and mean bias error for profile 8, although there the structure is not as well represented as in profile 7. It seems that the underestimation of temperature in WRF does not have a high influence on relative humidity, meaning that also specific humidity must be lower in the model than in the observations, which is probably due to reduced latent heat flux in case of more sea ice.

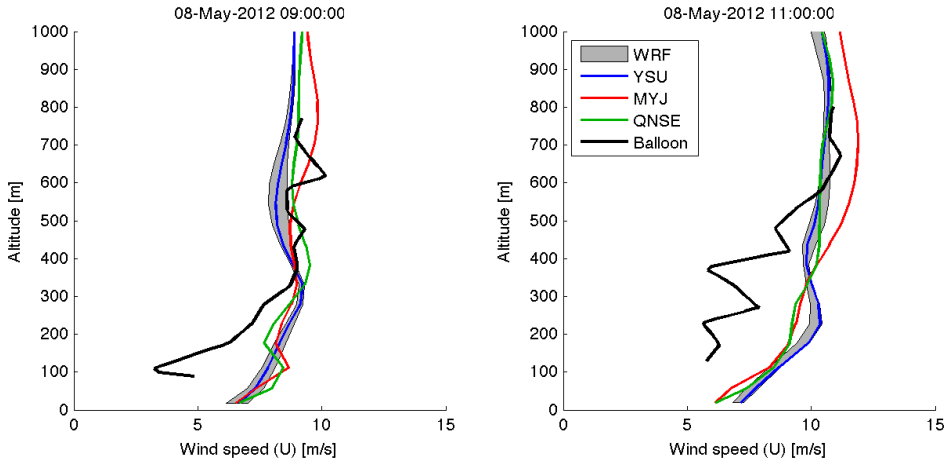

Figure 4.8: Observed and modelled wind (u) profiles. Grey band and colours as in Figure 4.3.

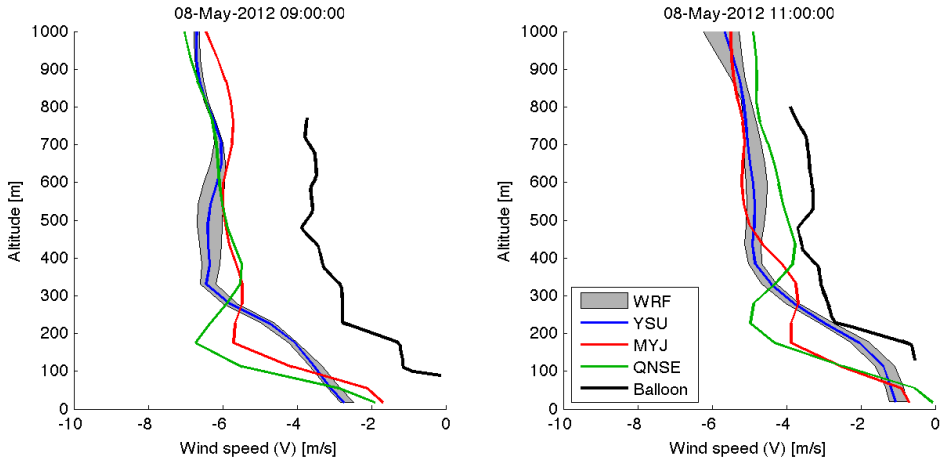

Figure 4.9: Observed and modelled wind (v) profiles. Grey band and colours as in Figure 4.3.

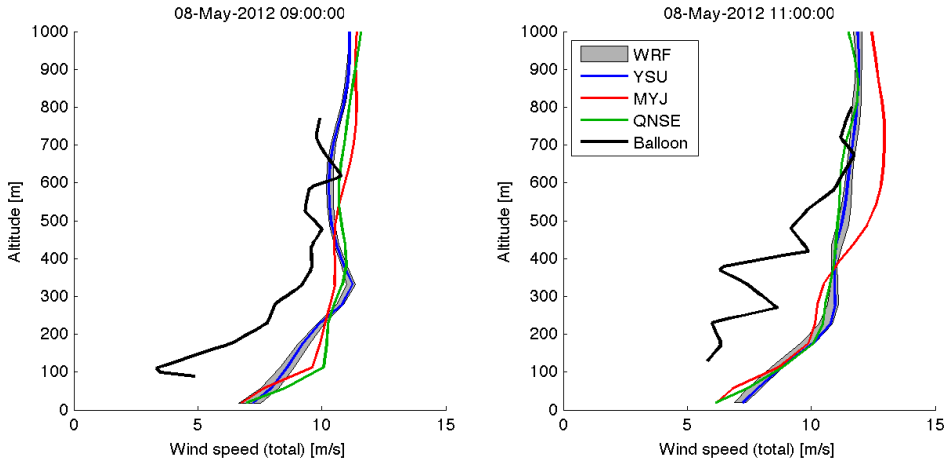

Figure 4.10: Observed and modelled wind (total) profiles. Grey band and colours as in Figure 4.3.

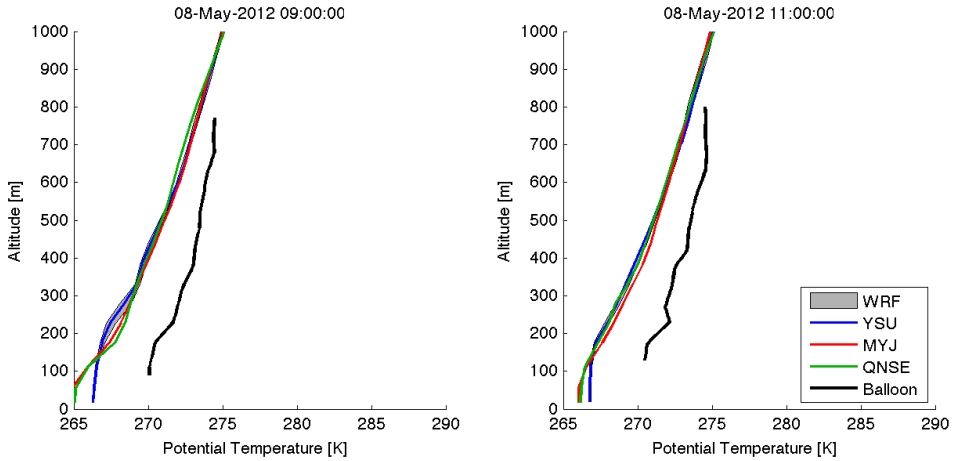

Figure 4.11: Observed and modelled potential temperature profiles. Grey band and colours as in Figure 4.3.

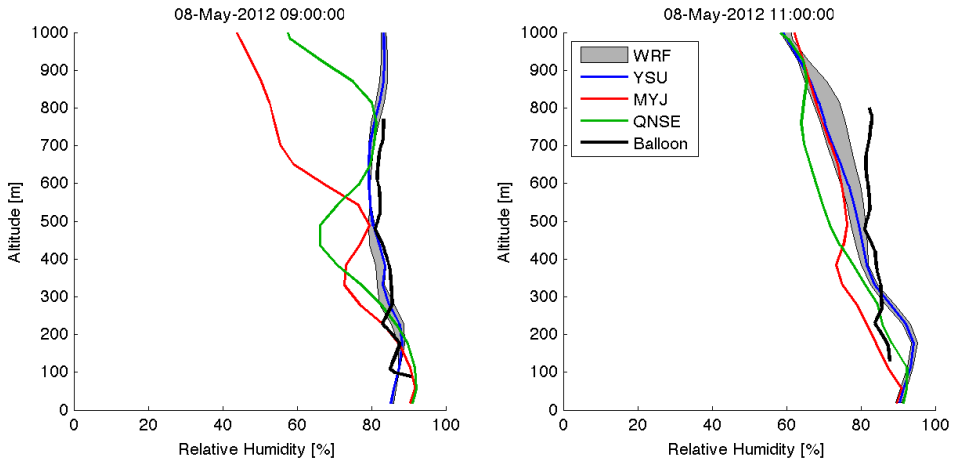

Figure 4.12: Observed and modelled relative humidity profiles. Grey band and colours as in Figure 4.3.

	Mean abs. error			Mean bias error		
Wind (u)	YSU	MYJ	QNSE	YSU	MYJ	QNSE
Profile 7	1.1715	0.9553	0.9004	0.3608	0.8022	0.6756
Profile 8	1.8154	2.1230	1.6786	1.5999	2.1230	1.4410
Average	**1.4935**	**1.5391**	**1.2895**	**0.9804**	**1.4626**	**1.0583**
Wind (v)						
Profile 7	2.6962	2.5932	2.9433	-2.6962	-2.5932	-2.9433
Profile 8	1.3181	1.4924	1.2470	-1.3181	-1.4924	-1.2470
Average	**2.0072**	**2.0428**	**2.0952**	**-2.0072**	**-2.0428**	**-2.0952**
Wind (total)						
Profile 7	1.5763	1.8533	1.9428	1.5574	1.8533	1.9428
Profile 8	2.0156	2.5336	1.8690	2.0156	2.5336	1.8185
Average	**1.7959**	**2.1935**	**1.9059**	**1.7865**	**2.1935**	**1.8807**
Pot. temp.						
Profile 7	2.7728	2.5933	2.7267	-2.7728	-2.5933	-2.7267
Profile 8	2.6798	2.4059	2.6801	-2.6798	-2.4059	-2.6801
Average	**2.7263**	**2.4996**	**2.7034**	**-2.7263**	**-2.4996**	**-2.7034**
Rel. humidity						
Profile 7	2.0766	11.2449	7.0854	-0.9256	-10.4236	-5.2106
Profile 8	5.3667	7.5444	9.2024	-2.4527	-7.5444	-8.7000
Average	**3.7216**	**9.3947**	**8.1439**	**-1.6892**	**-8.9840**	**-6.9553**

Table 4.2: Mean absolute error and mean bias error for the three boundary layer schemes in model run 2.

4.4 Timeseries

To analyse the performance of WRF over the time of the simulation period, timeseries were extracted from the model at the locations of three weather stations situated in Ny Ålesund, Verlegenhuken and Hopen. The locations are depicted in Figure 4.13. The weather station in Ny Ålesund is run by the Alfred Wegener Institute (AWI) and the Polar Institute Paul Emile Victor (IPEV), and takes measurements every minute. The stations in Verlegenhuken and Hopen are run by the Norwegian Meteorological Institute (met.no) and take measurements every six hours. Winds are measured 10m above ground, while temperature and relative humidity are measured 2m above ground. In order to get comparable correlation coefficients, the timeseries from Ny Ålesund was interpolated to 6h intervals. Likewise, the timeseries produced by WRF, which had a temporal resolution between 1s and 20s, depending on the time step, were interpolated to 6h intervals. The stations in Ny Ålesund and Verlegenhuken were included in the third domain of the first model run, while the station on Hopen was included in the third domain of the second model run.

The meteorological timeseries are generally well reproduced by WRF. The correlation is high and the p value is below 0.01 for every parameter and every station, meaning that all the correlations are statistically significant different from 0. Temperature is the

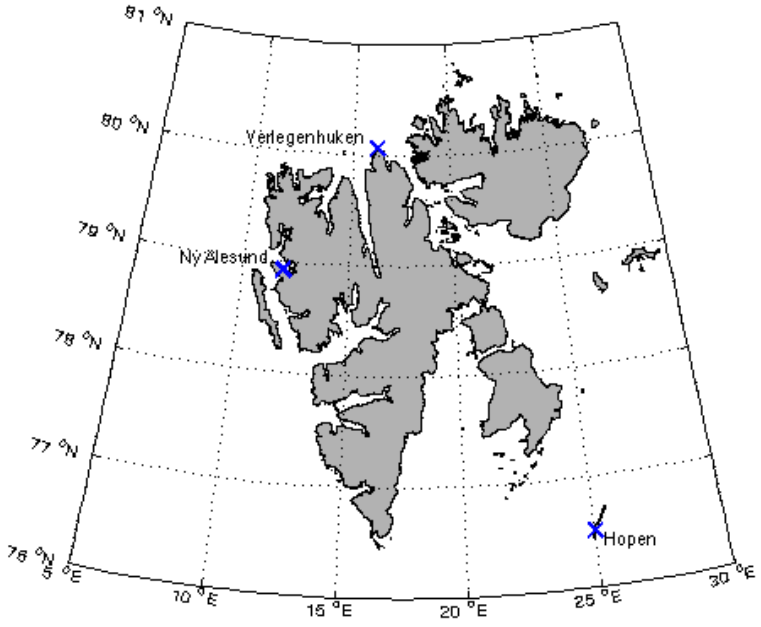

Figure 4.13: Locations of the weather stations.

parameter that has the highest correlation for most of the stations and schemes. It has however also quite a large bias. All the schemes overestimate temperature in Ny Ålesund and Verlegenhuken (especially the very low temperatures) and highly underestimate it on Hopen. On Hopen, this might be connected to fog that occurred in reality but remained unrepresented in the model, together with the fact that seaice was probably overrepresented in this area. Fog could also explain the lower daily variation in the observations compared to the model timeseries. For temperature, the MYJ scheme has the highest correlation, while the YSU scheme has the least mean absolute error and the least bias.

All the schemes show very strong southerly winds on 6 May 2011 in Ny Ålesund, which did not occur in reality. Otherwise, the winds are very reasonably reproduced by WRF, except for a small overestimation of the u component on Hopen in the end of the period. The QNSE scheme has the highest correlation for total wind speed as well as the lowest mean absolute error and bias.

Relative humidity is the parameter with the lowest correlation between the model and the observations. Especially remarkable are the values exceeding 100% on Hopen around 4 May and 7 May. The problem might be caused by an overestimation of atmospheric pressure, which leads to higher vapour pressure when calculating relative humidity from the mixing ratio. The QNSE scheme correlates best with the observations and has the least mean absolute error, but the YSU scheme shows a lower bias.

4.4.1 Wind roses

Figure 4.17 to 4.19 show wind roses for the different weather stations and the three ABL schemes at the given location. The main wind direction in Ny Ålesund is northwesterly and southeasterly, following the direction of Kongsfjorden, where Ny Ålesund is located. In WRF, the winds are turned by around 30° clockwise and the wind speeds of the northwesterly winds are much higher. Furthermore, there is a strong southerly component that cannot be found in the observations. This corresponds to the positive peak in the v component in Figure 4.14 on 6 May that was mentioned above. In Verlegenhuken, the winds are mainly southeasterly. There is also a smaller component from the southwest, but almost no winds from the northern two quadrants. In contrast, all the schemes in WRF have a strong northwesterly component with high wind speeds. This peak can be found on the evening of 8 May in the original data of u and v (not shown), where u was around 5m/s and v reached under -10m/s for a short period. Unfortunately, it got lost in the interpolation to 6h intervals. On Hopen, the observations reveal main wind directions from the southwest and the northeast. In WRF, the component from the northeast is almost completely missing, and the southwesterly component is underestimated in proportion as well as in speed. Winds coming from the north are overrepresented instead. This can also be seen in the negative bias of the v component in Table 4.3.

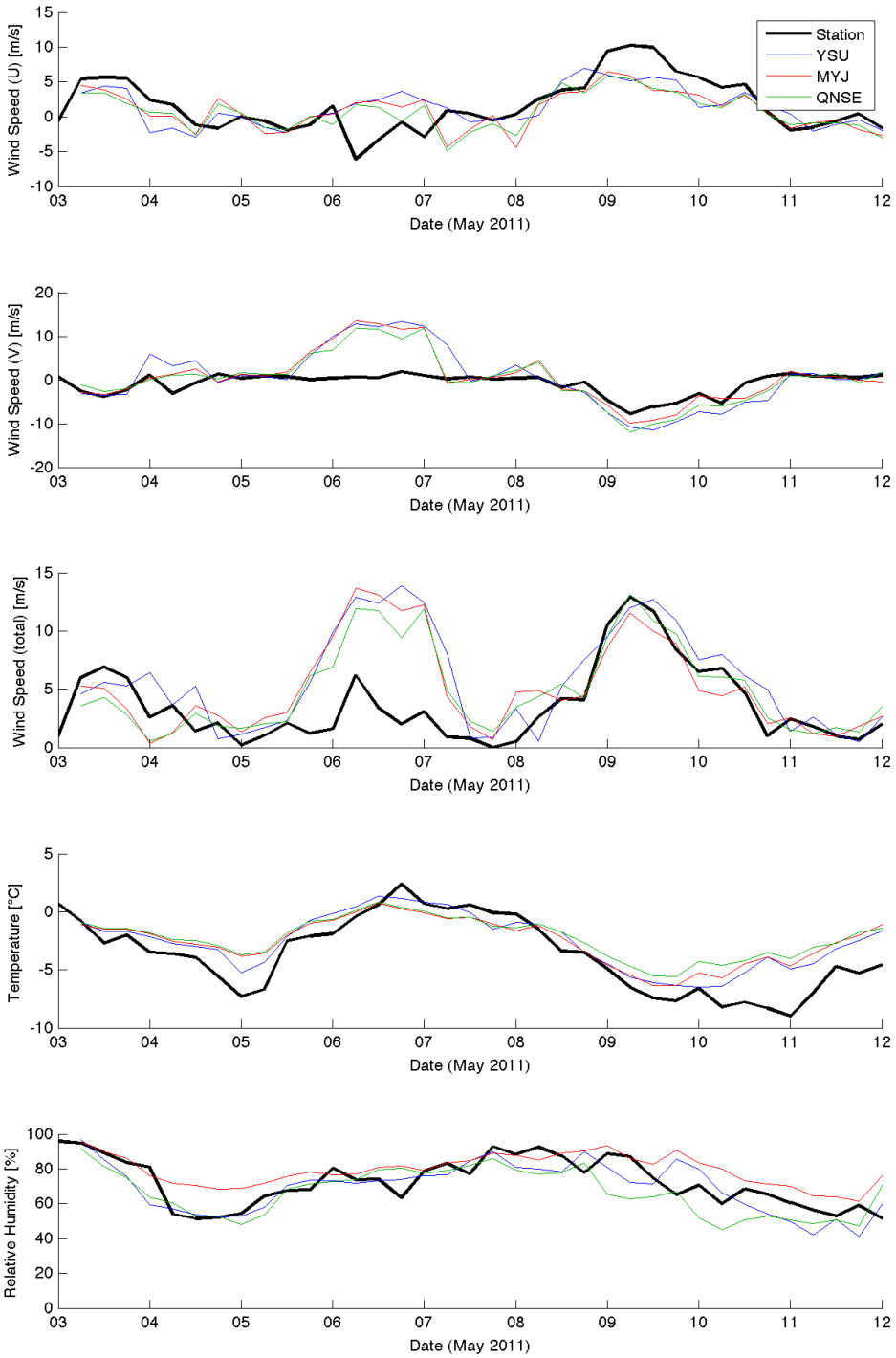

Figure 4.14: Observed and modelled timeseries for Ny Ålesund. The timeseries of the three ABL schemes are in colour, the observed timeseries is in black.

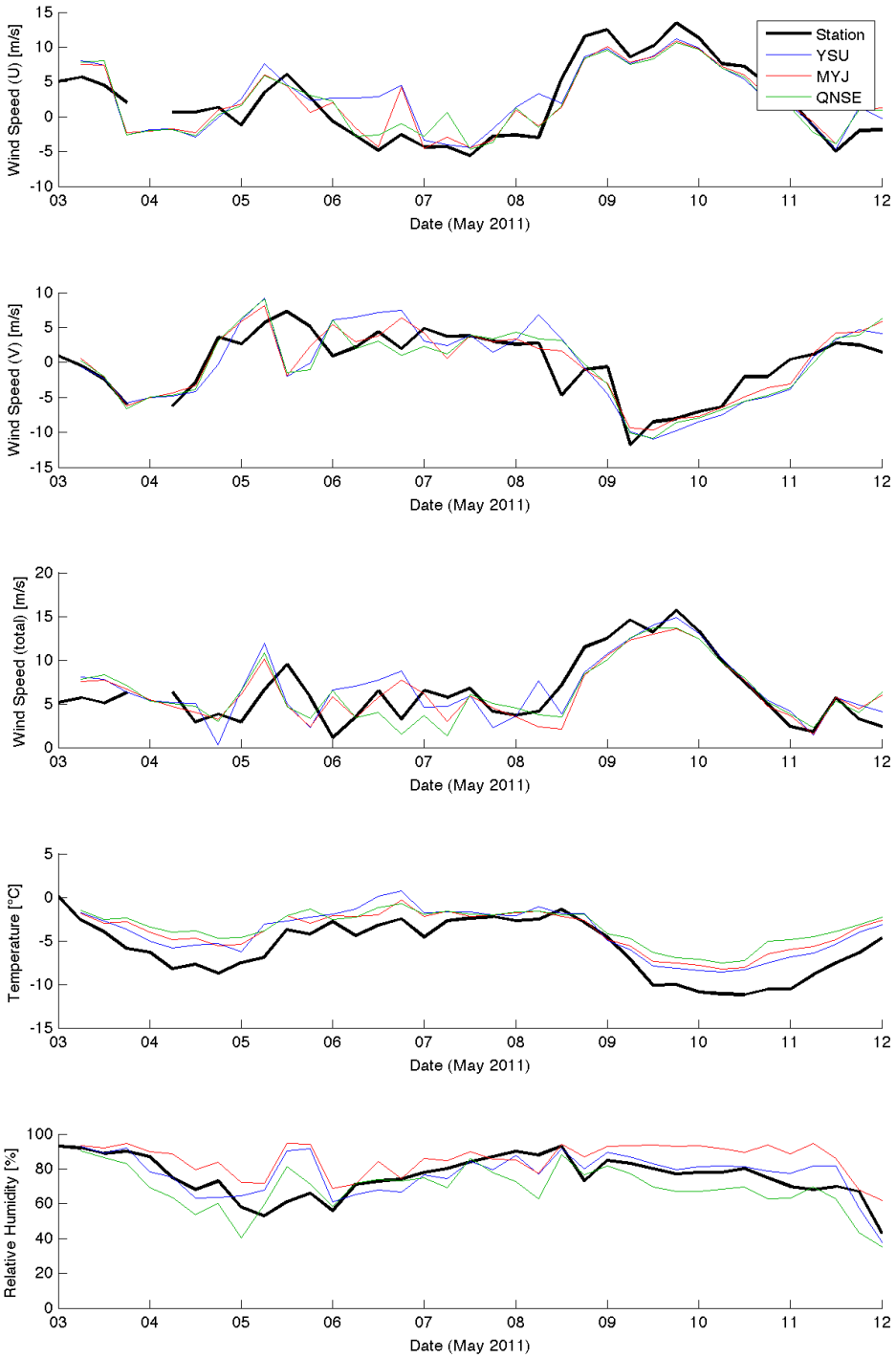

Figure 4.15: Observed and modelled timeseries for Verlegenhuken. Colours as in Figure 4.14.

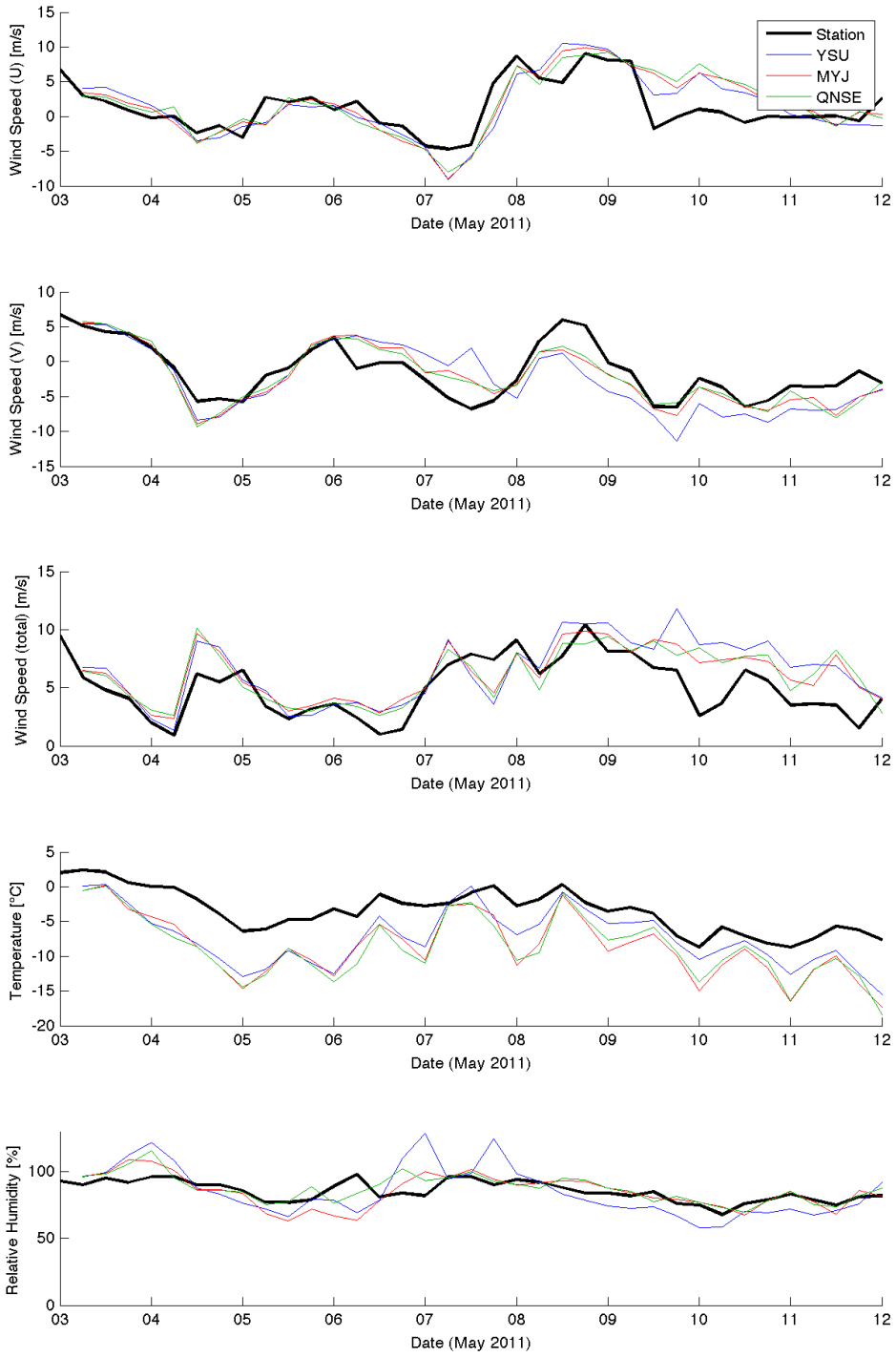

Figure 4.16: Observed and modelled timeseries for Hopen. Colours as in Figure 4.14.

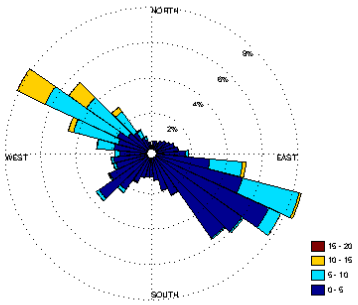

(a) AWIPEV station

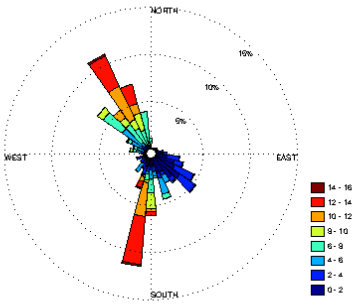

(b) YSU scheme

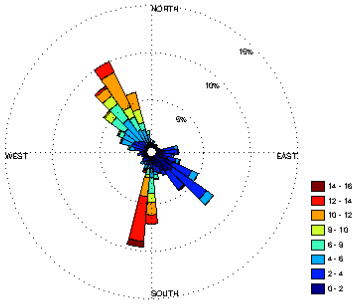

(c) MYJ scheme

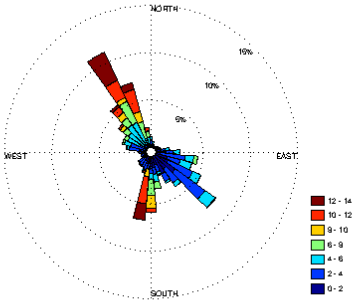

(d) QNSE scheme

Figure 4.17: Observed and modelled wind roses for Ny Ålesund in the period 3 May 2011 00:00 UTC to 12 May 2011 00:00 UTC. Colours indicate wind speed (m/s).

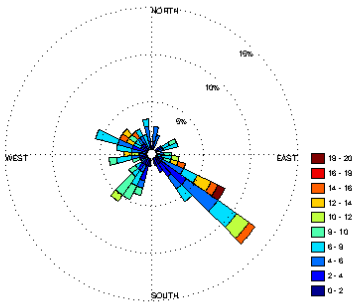

(a) Met.no station

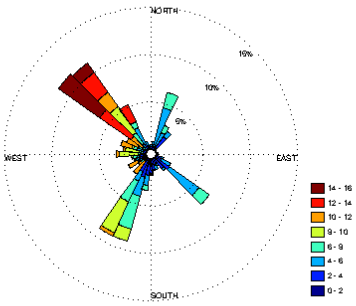

(b) YSU scheme

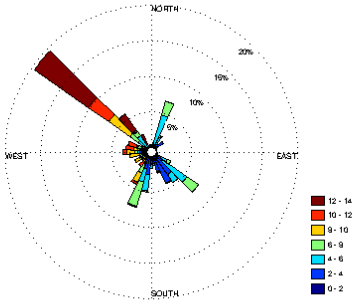

(c) MYJ scheme

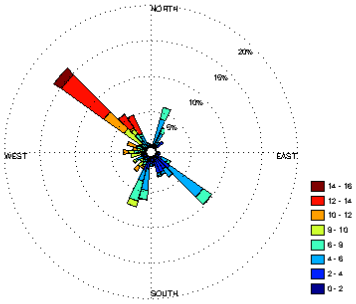

(d) QNSE scheme

Figure 4.18: Observed and modelled wind roses for Verlegenhuken in the period 3 May 2011 00:00 UTC to 12 May 2011 00:00 UTC. Colours indicate wind speed (m/s).

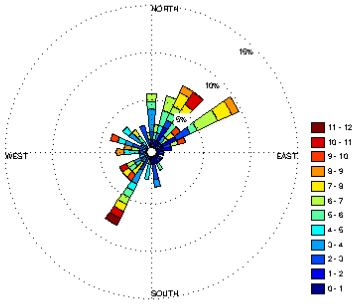

(a) Met.no station

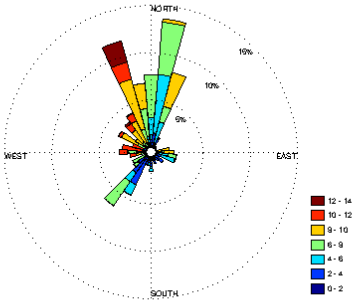

(b) YSU scheme

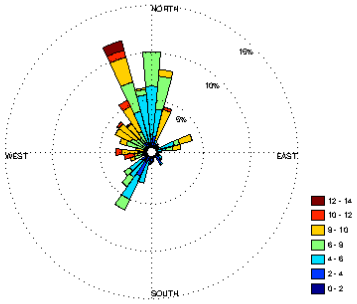

(c) MYJ scheme

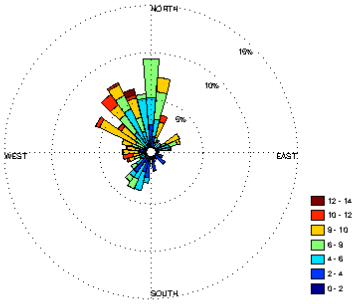

(d) QNSE scheme

Figure 4.19: Observed and modelled wind roses for Hopen in the period 3 May 2011 00:00 UTC to 12 May 2011 00:00 UTC. Colours indicate wind speed (m/s).

	Correlation coeff.			**Mean abs. error**			**Mean bias error**		
Wind (u)	YSU	MYJ	QNSE	YSU	MYJ	QNSE	YSU	MYJ	QNSE
Ny Ålesund	0.651	0.640	0.677	2.232	2.319	2.306	-0.281	-0.698	-0.905
Verlegenhuken	0.817	0.895	0.896	2.601	2.043	2.162	0.614	0.083	0.006
Hopen	0.782	0.770	0.729	2.142	2.122	2.224	0.253	0.488	0.541
Average	0.750	0.768	0.767	2.325	2.161	2.231	0.195	-0.043	-0.119
Wind (v)									
Ny Ålesund	0.724	0.691	0.750	3.681	2.898	2.938	1.449	1.534	1.068
Verlegenhuken	0.786	0.829	0.799	2.662	1.916	2.233	0.024	0.159	-0.215
Hopen	0.715	0.840	0.849	2.775	1.838	1.734	-1.003	-0.571	-0.480
Average	0.742	0.787	0.799	3.039	2.218	2.302	0.157	0.374	0.125
Wind (total)									
Ny Ålesund	0.596	0.527	0.646	2.697	2.528	2.280	2.149	1.445	1.317
Verlegenhuken	0.750	0.788	0.777	2.068	1.778	1.922	0.361	-0.141	-0.163
Hopen	0.691	0.758	0.681	1.997	1.659	1.702	1.508	1.238	1.082
Average	0.679	0.691	0.701	2.254	1.988	1.968	1.340	0.847	0.745
Temperature									
Ny Ålesund	0.924	0.891	0.911	1.382	1.642	1.901	1.146	1.220	1.513
Verlegenhuken	0.939	0.944	0.921	1.915	2.039	2.538	1.873	1.982	2.503
Hopen	0.809	0.867	0.815	3.748	5.031	5.104	-3.684	-5.031	-5.104
Average	0.891	0.901	0.882	2.348	2.904	3.181	-0.222	-0.610	-0.362
Rel. humidity									
Ny Ålesund	0.785	0.802	0.725	7.635	8.508	9.132	-2.607	7.321	-5.371
Verlegenhuken	0.706	0.624	0.727	6.531	11.219	8.868	1.792	10.280	-6.431
Hopen	0.620	0.614	0.684	10.984	6.752	5.869	-0.148	-0.192	2.253
Average	0.704	0.680	0.712	8.383	8.826	7.956	-0.321	5.803	-3.183
Total avg.	**0.753**	**0.765**	**0.772**						

Table 4.3: Correlation coefficient, mean absolute error and mean bias error for the three boundary layer schemes at the three weather stations.

5 Discussion

5.1 Wind

WRF had a tendency to overestimate surface wind speeds, especially in case of strong winds (see profile 2 and 3 in Figure 4.3 to 4.5 and profile 1 in Figure 4.8 to 4.10). These results correspond to a study conducted by Claremar et al. (2012), which compared the Polar WRF model to observations from AWS placed on three Svalbard glaciers and found the same tendency of WRF to overestimate the highest wind speeds. However, since their AWS measured wind speed at a height below 10m, they used a correction based on Monin-Obukhov theory to calculate wind speed at 10m. This correction was constant and might, as mentioned by the authors, have led to too low wind speeds in case of more neutral stability, which is expected at high wind speeds. Nevertheless, the findings are supported by studies made by Kilpeläinen et al. (2011) and Kilpeläinen et al. (2012), which showed that wind speeds in Kongsfjorden were overestimated by WRF in the lowest levels. Kilpeläinen et al. (2012) also found that the average modelled low level jet was deeper and stronger than the average observed low level jet. In this study, the model did not show any low level jet, even though it was found twice in the observations.

5.2 Temperature

WRF highly underestimated the temperatures measured over sea ice to the east of Svalbard, in particular at the surface. As mentioned in Section 4.3, the bias is most probably due to an overrepresentation of sea ice in the WRF model setup. Sensitivity tests including one model run with complete sea ice coverage and one model run with open sea only confirmed that temperatures at low levels strongly depend on whether sea ice is present or not. In further investigations it would therefore make sense to include fractional sea ice in the model, maybe even together with varying sea ice and SST.

Moreover, WRF did not manage to capture the inversions observed in profile 2 and 3 in Figure 4.6. This problem has been encountered before. Mölders and Kramm (2010), who ran WRF for a five day cold weather period in Alaska, found that WRF has difficulties in capturing the full strength of the surface temperature inversion that was observed during that period. Similar results were found in the study by Kilpeläinen et al. (2012), where WRF reproduced only half the amount of inversions that were found in the observations, and thereby often underestimated its depth and strength. Mölders and Kramm (2010) suggest that, since low wind speeds to no wind are favourable for inversion formation, WRF's overestimation of wind speed might partly explain the difficulties in capturing (the strength of) inversions. Also, elevated inversions are often connected to

low level jets (Andreas et al., 2000), thus the difficulties in capturing inversions might explain the absence of low level jets.

5.3 Relative humidity

Studies by Steeneveld et al. (2008) and Mayer et al. (2012a) showed that local ABL schemes produced shallower and moister boundary layers than nonlocal schemes. In this study, all the schemes mostly showed a shallower and moister ABL than the observations. However, the two local schemes MYJ and QNSE in average produced lower vertical relative humidity profiles than the nonlocal YSU scheme (see bias in Table 4.1 and 4.2). In contrast, for the timeseries it is the MYJ scheme that most often showed the highest relative humidity, while the QNSE scheme had the lowest relative humidity (bias in Table 4.3). WRF generally had the most difficulties in reproducing the relative humidity profiles in the cases with strong winds (profile 2 and 3 in Figures 4.5 and 4.7). It highly underestimated relative humidity at the location of the low level jet.

5.4 Parameterisation schemes

The YSU scheme without doubt showed the best overall performance when compared to the CMET balloon profiles. This stands in contrast to the results found by Kilpeläinen et al. (2012), where the YSU scheme yielded the largest errors in the vertical profiles. When looking at the timeseries, the MYJ and the QNSE scheme showed smaller absolute errors than the YSU scheme for all parameters except temperature. The QNSE scheme yielded the smallest absolute errors for relative humidity and total wind speed, while the MYJ scheme was better considering the u and v component of the wind separately. Additionally, the average correlation coefficient for each parameter was highest for either the MYJ or the QNSE scheme, the QNSE scheme having the highest correlation coefficient in total. This agrees with the results found by Claremar et al. (2012), which showed that the QNSE scheme outperformed the MYJ scheme when compared to measurements from AWS. It leads us to the conclusion that the QNSE scheme is especially powerful at the lower levels, where the timeseries were measured, while having more difficulties reproducing vertical profiles. The YSU scheme shows the best performance for the vertical profiles. However, the differences between the schemes in total were very small, and, moreover, the observational period was rather short, including only seven days. The statistical significance of the results found might therefore be limited.

6 Future work

The results presented in Section 4.3 show that WRF, when compared to vertical profiles measured over sea ice, underestimated temperature and overestimated wind speed, especially at low levels. These results suggest to have a closer look at the implementation of sea ice into WRF in further investigations. Even though the sea ice flag from the ECMWF data seems to agree fairly well with the real sea ice flag seen on a satellite picture that was taken at that time, areas of polynyas and leads that can be recognised on the satellite picture were represented as homogeneous sea ice in the model. One option is to remove excessive sea ice manually, as, e.g., in Mayer et al. (2012b). Another or additional option is to use fractional sea ice. In the ECMWF data, grid cells with leads and polynyas are represented as only partly covered by sea ice (a fraction smaller than one). Such a fractional sea ice option is available for WRF version 3.1.1 and higher. Yet, in this study we ran the model without the option of fractional sea ice and therefore assumed that each grid cell within the sea ice flag was fully covered by sea ice. This could explain the errors in the profiles of Section 4.3 and needs to be further investigated. However, it is difficult to implement fractional sea ice accurately. The amount of sea ice in a grid cell is varying in time through sea ice formation, break up and drifting, where drifting is the dominant process in late spring. Therefore, it is not advisable to leave the sea ice field constant during the simulation time in case the fractional sea ice option is used. However, since WRF is a meteorological model, it does not include modelling of ocean currents and hence drifting of sea ice. The presence of sea ice only depends on whether the SST is above or below the freezing point of water. An option to overcome this problem is to update the sea ice field and the SST in a certain interval (e.g., six hours) with data from observations or reanalyses, as in Kilpeläinen et al. (2012).

Polar WRF was developed especially for the Arctic and Antarctic, with a selection of physical parameterisations best suited for polar regions. In further investigations it might be interesting to see whether Polar WRF performs better than the standard WRF in our case. However, one of the major advantages of Polar WRF was the treatment of fractional sea ice, which has not been available before, but is now also included in the standard WRF. Accordingly, studies by Kilpeläinen et al. (2012) showed that the differences between the standard WRF version 3.1.1 and its corresponding polar version were marginal. Standard WRF even captured the wind and temperature profiles slightly better than Polar WRF.

Finally, it would probably also be better to look at specific humidity in future analyses instead of (or in addition to) relative humidity, since relative humidity might be biased through pressure and temperature.

7 Acknowledgements

I would like to thank Lars Robert Hole for accepting me as an intern at met.no. I am very happy to have been given the chance to work in Bergen and participate in this project. Also thanks for the many helpful talks and discussions and the suggestion to apply for a course on Svalbard. Thanks to Paul Voss for the supportive discussions via skype and the help in writing the report. Thanks to Marius Jonassen for helping in getting familiar with WRF and its brother WPS and for always having an answer and being ready to help when there was a problem with the model. Thanks to Siegrid Debatin from AWIPEV for providing us with radiosonde and weather station data from Ny Ålesund. Big thanks to Aslaug Valved and Aurora Stenmark for being awesome friends and WRF buddies. Takk til Bergen for et fantastisk halvt år.

Bibliography

E. L. Andreas, K. J. Claffey, and A. P. Makshtas. Low-level atmospheric jets and inversions over the western weddell sea. *Boundary-Layer Meteorology*, 97:459–486, 2000.

R. Bintanja, R. G. Graversen, and W. Hazeleger. Arctic winter warming amplified by the thermal inversion and consequent low infrared cooling to space. *Nature Geoscience*, 4:758–761, 2011.

D. H. Bromwich, K. M. Hines, and L.-S. Bai. Development and testing of polar weather research and forecasting model: 2. arctic ocean. *J. Geophys. Res.*, 114:D08122, 2009.

F. Chen and J. Dudhia. Coupling an advanced land-surface/ hydrology model with the penn state/ ncar mm5 modeling system. part i: Model description and implementation. *Mon. Wea. Rev.*, 129:569–585, 2001.

B. Claremar, F. Obleitner, C. Reijmer, V. Pohjola, A. Waxegård, F. Karner, and A. Rutgersson. Applying a mesoscale atmospheric model to svalbard glaciers. *Advances in Meteorology*, 2012:22 pages, 2012. Article ID 321649.

J. Dudhia. Numerical study of convection observed during the winter monsoon experiment using a mesoscale two-dimensional model. *J. Atmos. Sci.*, 46:3077–3107, 1989.

K. M. Hines and D. H. Bromwich. Development and testing of polar weather research and forecasting (wrf) model. part i: Greenland ice sheet meteorology*. *Mon. Wea. Rev.*, 136:1971–1989, 2008.

S.-Y. Hong, J. Dudhia, and S.-H. Chen. A revised approach to ice microphysical processes for the bulk parameterization of clouds and precipitation. *Mon. Wea. Rev.*, 132:103–120, 2004.

S.-Y. Hong, Y. Noh, and J. Dudhia. A new vertical diffusion package with an explicit treatment of entrainment processes. *Mon. Wea. Rev.*, 134:23182341, 2006.

J. T. Houghton, Y. Ding, D. J. Griggs, M. Noguer, P. J. van der Linden, X. Dai, K. Maskel, C. A. Johnson, and Eds. *Climate Change 2001: The Scientific Basis.* Cambridge University Press, 2001.

Z. I. Janjic. The step-mountain coordinate: physical package. *Mon. Wea. Rev.*, 118: 1429–1443, 1990.

Z. I. Janjic. The surface layer in the ncep eta model. In *Eleventh Conference on Numerical Weather Prediction*, pages 354–355, Norfolk, VA, 19-23 August 1996. American Meteorological Society.

Z. I. Janjic. Nonsingular implementation of the melloryamada level 2.5 scheme in the ncep meso model. *NCEP Office Note*, No. 437:61 pp, 2002.

J. S. Kain. The kain-fritsch convective parameterization: An update. *J. Appl. Meteor.*, 43:170–181, 2004.

T. Kilpeläinen, T. Vihma, and H. Ólafsson. Modelling of spatial variability and topographic effects over arctic fjords in svalbard. *Tellus A*, 63(2):223–237, 2011.

T. Kilpeläinen, T. Vihma, M. Manninen, A. Sjöblom, E. Jakobson, T. Palo, and M. Maturilli. Modelling the vertical structure of the atmospheric boundary layer over arctic fjords in svalbard. *Q. J. R. Meteorol. Soc.*, 2012.

G. Livik. An observational and numerical study of local winds in kongsfjorden, spitsbergen, 2011. Master Thesis at the University of Bergen.

J. Lu and M. Cai. Quantifying contributions to polar warming amplification in an idealized coupled general circulation model. *Climate Dynamics*, 34:669–687, 2010.

E. Mäkiranta, T. Vihma, A. Sjöblom, and E.-M. Tastula. Observations and modelling of the atmospheric boundary layer over sea-ice in a svalbard fjord. *Boundary-Layer Meteorology*, 140:105–123, 2011.

S. Mayer, A. Sandvik, M. Jonassen, and J. Reuder. Atmospheric profiling with the uas sumo: a new perspective for the evaluation of fine-scale atmospheric models. *Meteorology and Atmospheric Physics*, 116:15–26, 2012a.

S. Mayer, M. Jonassen, A. Sandvik, and J. Reuder. Profiling the arctic stable boundary layer in advent valley, svalbard: Measurements and simulations. *Boundary-Layer Meteorology*, 143:507–526, 2012b.

G. L. Mellor and T. Yamada. Development of a turbulence closure model for geophysical fluid problems. *Rev. Geophys. Space Phys.*, 20:851–875, 1982.

A. C. Mentzoni. Flexpart validation with the use of cmet balloons, 2011. Master Thesis at the University of Bergen.

E. J. Mlawer, S. J. Taubman, P. D. Brown, M. J. Iacono, and S. A. Clough. Radiative transfer for inhomogeneous atmospheres: Rrtm, a validated correlated-k model for the longwave. *J. Geophys. Res.*, 102:16663–16682, 1997.

N. Mölders and G. Kramm. A case study on wintertime inversions in interior alaska with wrf. *Atmospheric Research*, 95(23):314–332, 2010.

P. O. G. Persson, C. W. Fairall, E. L. Andreas, P. S. Guest, and D. K. Perovich. Measurements near the atmospheric surface flux group tower at sheba: Near-surface conditions and surface energy budget. *J. Geophys. Res.*, 107:8045–8079, 2002.

E. E. Riddle, P. B. Voss, A. Stohl, D. Holcomb, D. Maczka, K. Washburn, and R. W. Talbot. Trajectory model validation using newly developed altitude-controlled balloons during the international consortium for atmospheric research on transport and transformations 2004 campaign. *J. Geophys. Res.*, 111:D23S57, 2006.

A. Rinke, K. Dethloff, J. Cassano, J. Christensen, J. Curry, P. Du, E. Girard, J.-E. Haugen, D. Jacob, C. Jones, M. Kltzow, R. Laprise, A. Lynch, S. Pfeifer, M. Serreze, M. Shaw, M. Tjernstrm, K. Wyser, and M. agar. Evaluation of an ensemble of arctic regional climate models: spatiotemporal fields during the sheba year. *Climate Dynamics*, 26:459–472, 2006.

W. Skamarock, J. Klemp, J. Dudhia, D. Gill, D. Barker, M. Duda, H. X. Y., and W. Wang. A description of the advanced research wrf version 3, 2008. NCAR/TN:475+STR.

G. J. Steeneveld, T. Mauritsen, E. I. F. de Bruijin, J. Vilà-Guerau de Arellano, G. Svensson, and A. A. M. Holtslag. Evaluation of limited-area models for the representation of the diurnal cycle and contrasting nights in cases-99. *J. Appl. Meteor. Climatol.*, 47: 869–887, 2008.

A. Stohl, G. Wotawa, P. Seibert, and H. Kromp-Kolb. Interpolation errors in wind fields as a function of spatial and temporal resolution and their impact on different types of kinematic trajectories. *J. Appl. Meteorol.*, 34:2149–2165, 1995.

A. Stohl, M. Hittenberger, and G. Wotawa. Validation of the lagrangian particle dispersion model flexpart against large-scale tracer experiment data. *Atmospheric Environment*, 32(24):4245–4264, 1998.

S. Sukoriansky, B. Galperin, and V. Perov. A quasi-normal scale elimination model of turbulence and its application to stably stratified flows. *Nonlinear Processes in Geophysics*, 13:9–22, 2006.

P. B. Voss, R. A. Zaveri, F. M. Flocke, H. Mao, T. P. Hartley, P. DeAmicis, I. Deonandan, G. Contreras-Jiménez, O. Martínez-Antonio, M. Figueroa Estrada, D. Greenberg, T. L. Campos, A. J. Weinheimer, D. J. Knapp, D. D. Montzka, J. D. Crounse, P. O. Wennberg, E. Apel, S. Madronich, and B. de Foy. Long-range pollution transport during the milagro-2006 campaign: a case study of a major mexico city outflow event using free-floating altitude-controlled balloons. *Atmos. Chem. Phys.*, 10:7137–7159, 2010.

P. B. Voss, L. R. Hole, E. Helbling, and T. Roberts. Continuous in-situ soundings in the arctic boundary layer: A new atmospheric measurement technique using controlled meteorological balloons. *Journal of Intelligent & Robotic Systems*, pages 1–9, 2012.